# Studies on Ni(II), Cu(II) and Zn(II) complexes with 2-aminobenzamide and some bioactive imidazole enzyme constituents

Jeyaprakash Dharmaraja, Paramasivam Subbaraj, Thirugnanasamy Esakkidurai & Sutha Shobana

➕ View supplementary material ↗

📅 Accepted author version posted online: 13 Oct 2015.
Published online: 03 Nov 2015.

✏️ Submit your article to this journal ↗

📊 Article views: 101

🔍 View related articles ↗

CrossMark View Crossmark data ↗

Taylor & Francis
Taylor & Francis Group

# Studies on Ni(II), Cu(II) and Zn(II) complexes with 2-aminobenzamide and some bioactive imidazole enzyme constituents

JEYAPRAKASH DHARMARAJA†, PARAMASIVAM SUBBARAJ‡,
THIRUGNANASAMY ESAKKIDURAI*‡ and SUTHA SHOBANA§

†Division of Chemistry, Faculty of Science and Humanities, Sree Sowdambika College of Engineering, Aruppukottai, India
‡Department of Chemistry, Devanga Arts College (Autonomous), Aruppukottai, India
§Department of Chemistry and Research Centre, Aditanar College of Arts and Science, Tiruchendur, India
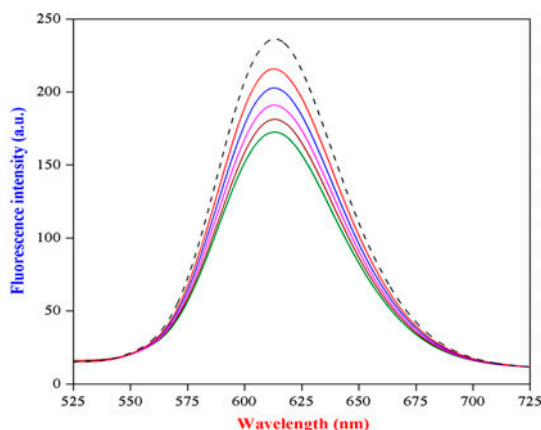
A series of Ni(II), Cu(II), and Zn(II) complexes of 2-aminobenzamide(2AB : L) and some imidazole enzyme constituents(B) viz., imidazole(him), benzimidazole(bim), histamine(hist), and L-histidine (his) have been synthesized and characterized using analytical and various spectral studies. Vibrational spectral data of the synthesized complexes reveal that the ligands bind with metal(II) ions through nitrogen and oxygen. The calculated *g*-tensor values of Cu(II) complexes suggest that the unpaired electron is localized in the $d_{x^2-y^2}$ orbital. The results obtained from the spectral studies confirm the distorted octahedral environment around the metal(II) ions. Their powder XRD indicates microcrystalline nature and SEM pictographs identify their uniform surface morphology. Cu(II) and Ni(II) complexes show biological, antioxidant, and DNA activities when compared to free 2-aminobenzamide. Equilibrium studies have been carried out pH-metrically in 50% (v/v) water–ethanol mixture at 37 °C and $I = 0.15$ mol dm$^{-3}$ NaClO$_4$. Analysis reveals the presence of certain heteroligand species viz., MLBH/MLB/MLB$_2$, in addition to various primary species. In MLB/ MLB$_2$ species, 2AB(L) binds with M(II) ions via N-amino and O-amido, whereas the ligands(B)

---

*Corresponding author. Emails: tesakkidurai.dac@gmail.com, devangaartscollege@gmail.com

him and bim are monodentate, hist and his are bi and tridentate, respectively. The stabilization parameters $\Delta \log K$, $\log X$, $\log X'$, and % RS clearly indicate all the heteroligand complexes have higher stabilities than their primary.

## 1. Introduction

Interaction of bioactive molecules which contain hard and soft donor N-, O-, and/or S-ligating sites with transition metal(II) ions to form the heteroligand complexes leads to the revolution of various physicochemical and biological properties in the living systems [1, 2]. Heteroligand complexes have been used as effective therapeutic agents in various medical and cosmetic fields [3, 4]. Benzamide and its substituted derivatives are widely used as drugs since they possess a broad spectrum of biological activities such as analgesics, antiprion, antiemetic, anthelmintic, antihypertensive, antidyskinetic, antibacterial, antifungal, antimalarial, antipsychotic, anti-inflammatory, antihistaminic, antileukotriene, antioxidative, antithrombotic, anticonvulsant, anti-HIV-1, and antihelicobacter pylori activities [5, 6]. Also, their derivatives (Epidepride, Fallypride, and Isoremoxipride) are widely used as high-affinity radioligands for PET (Positron Emission Tomography) imaging of dopamine D2/D3 receptors in the human brain [7]. They act as potent and selective histone deacetylase enzyme (HDAC) and poly(ADP-ribose)polymerase (PARP) inhibitors. The factor $X_a$ ($FX_a$) is a trypsin-like serine endopeptidase, which converts prothrombin zymogen into its active thrombin form in the blood coagulation cascade [8]. 2-Aminobenzamide (Anthranilamide: 2AB) and its derivatives are widely used as selective and potent $FX_a$ inhibitors [8], i.e. they have been employed as novel anticoagulant drugs for curing thromboembolic disorders. Also, they are used as fluorescent reagents for labeling of oligosaccharides in HPLC technique for analysis of protein glycosylation [9].

Metals are essential trace elements to humans, higher animals, and plants [10]. Heterocyclic imidazole ring moieties containing bioactive organic groups can potentially mimic the binding sites and catalytic activities of numerous enzymes [11]; they also possess a wide range of pharmacological activities. Imidazole nitrogen donor of histidine residue is the most common binding site of many metalloproteins and so shows a profound effect on biological actions [10, 12]. A part of the nucleotide portion of vitamin $B_{12}$ has benzimidazole and these ring moieties are widely used in modern medicinal and clinical fields [13]. Investigations on heteroligand complexes with nucleic acids are important for the design and development of genetic material structures and functions, metallodrugs, and bioactive agents in chemotherapeutic agents, footprinting agents, spectroscopic probes, molecular photoswitches, and diagnostic tools in medical fields [14]. Oxidative cleavage interactions of DNA in photochemical methods have been applied in the field of photodynamic therapy of cancer [15].

In continuation of our recent reports [16–20], the major goal of the present work is to synthesize Ni(II), Cu(II), and Zn(II) complexes from 2-aminobenzamide (2AB : L) and some imidazoles ligand(B) viz., imidazole (him), benzimidazole (bim), histamine (hist), and L-histidine (his) (figure 1). The synthesized complexes were structurally characterized by analytical and spectral techniques. *In vitro* biological and antioxidant activities of free 2AB
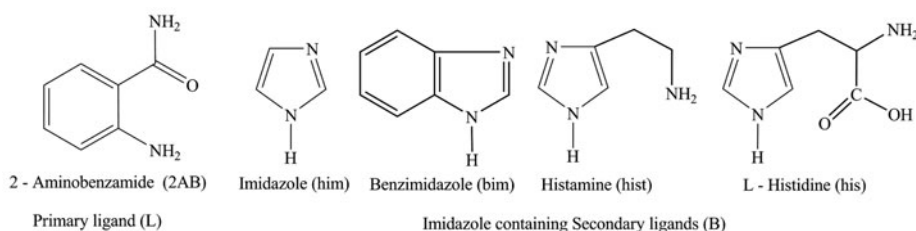
Figure 1. Structure of primary and secondary ligands.

(L) and its heteroligand complexes have also been studied and the results were compared with the standard controls. The binding and oxidative cleavage interactions of heteroligand complexes with CT-DNA were investigated. In addition, the solution equilibria of primary and heteroligand complexes have been studied pH-metrically in 50% (v/v) water–ethanol mixture containing $I = 0.15$ mol dm$^{-3}$ (NaClO$_4$) at 37 °C.

## 2. Experimental

### 2.1. *Materials and physical measurements*

All the chemicals and solvents used in this work were extra pure analytical grade and purchased from Sigma-Aldrich and Fluka (Puriss) products without further purification. The solvents used for the preparation and physical measurements were purified according to the literature methods [21]. CT-DNA was purchased from Genie, Bangalore. Carbonate-free NaOH solution (0.3 M) was prepared from a Titrisol (Merck) solution and its concentration was standardized against standard potassium hydrogen phthalate solution by appropriate Gran titrations [22]. Metal perchlorates and other solutions were prepared and estimated as described earlier [16, 18]. Triply distilled CO$_2$-free water with specific conductance equal to $(1.81 \pm 0.1 \ \Lambda^{-1} \ cm^{-1})$ was used for the preparation of all solutions. Melting points (m.p.) of the complexes were determined on a Gallenkamp apparatus in an open glass capillary tube and are uncorrected. Micro-analytical data were performed on an Elementar Vario EL III CHNS analyzer and the metal(II) content in the complexes was estimated gravimetrically by the standard ammonium oxalate method. Molar conductance ($\Lambda_m$) of the complexes $(1 \times 10^{-3}$ mol solution in DMSO) was measured using an Elico CM 180 conductivity bridge with a KCl solution as calibrant. Fast-atom bombardment mass spectra (FAB-MS) were recorded using a VGZAB-HS spectrometer in a 3-nitrobenzylalcohol matrix. Magnetic susceptibility measurements were carried out on a Gouy balance at room temperature using mercuric tetra(thiocyanato)cobaltate(II) as the calibrant and the diamagnetic corrections were applied in compliance with the Pascal's constant [23]. Electronic spectra (200–1100 nm) were measured using a Hitachi U-2000 double-beam spectrophotometer. IR spectra were recorded as KBr disks on a JASCO FT/IR-410 spectrometer (400–4000 cm$^{-1}$). The X-band EPR spectrum of Cu(II) complexes at room temperature and liquid nitrogen conditions were recorded on a Varian ESR spectrometer using DPPH as internal standard. The proton NMR spectral observation of the diamagnetic Zn(II) complexes was carried out in DMSO-d$_6$ at room temperature using tetramethylsilane (TMS) as internal standard on a

Perkin Elmer R-32 spectrometer. Powder X-ray diffraction (PXRD) patterns were recorded on a Bruker AXS D8 advance powder X-ray diffractometer (Detector: Si(Li)PSD, X-ray source: Cu, wavelength: 1.5406 Å). DNA binding was recorded in 50% (v/v) water–ethanol mixture on a Hitachi U-2000 double-beam spectrophotometer. The 3-D molecular modeling of the synthesized heteroligand Ni(II) complexes was carried out on the CS Chem 3-D Ultra Molecular Modeling and Analysis Program [24] and the structure of the complexes were constructed using Chem Draw Ultra 11.0.

## 2.2. *General procedure for the synthesis of heteroligand MLB complexes*

2-Aminobenzamide (0.136 g, 1 mmol) was completely dissolved in hot 50% (v/v) water–ethanol mixture (10 mL) and added drop by drop to the metal(II) acetate salts [Ni(CH$_3$COO)$_2$·4H$_2$O (0.250 g, 1 mmol) or Cu(CH$_3$COO)$_2$·H$_2$O (0.200 g, 1 mmol) or Zn(CH$_3$COO)$_2$·2 H$_2$O (0.220 g, 1 mmol)] in an aqueous (10 mL) medium and stirred at room temperature for 2–3 h. To this solution, aqueous solution (10 mL) of imidazole (0.070 g, 1 mmol) or benzimidazole (0.120 g, 1 mmol) or histamine (0.110 g, 1 mmol) or L-histidine (0.160 g, 1 mmol) were added and refluxed for 6–8 h on a water bath. The reaction mixture was maintained at pH 7.4 by adding a few drops of aqueous Na$_2$CO$_3$ solution. The resulting solution was reduced to 1/3 of its original volume by water bath and kept aside. On standing, the solid complexes were collected by *vacuum* filtration, washed several times with cold and hot water, ethanol and anhydrous ether. The complexes were obtained as powders, dried in air, and stored in *vacuo* over anhydrous CaCl$_2$ at room temperature (Yield: 60–75%).

## 2.3. *Pharmacological studies*

### 2.3.1. **Biological activity**. The *in vitro* biological activities of free 2-aminobenzamide and its M(II)–2AB(L)–him/bim/hist/his(B) complexes were tested against some pathogenic bacterial species such as *Escherichia coli*, *Staphylococcus saphyphiticus*, *Staphylococcus aureus,* and *Pseudomonas aeruginosa* using Mueller-Hinton nutrient agar and fungal species such as *Aspergillus niger*, *Enterobacter species,* and *Candida albicans* using potato dextrose agar as the medium by modified well diffusion technique [25]. The test solution of free 2AB(L) and its heteroligand complexes ($3 \times 10^{-3}$ mol) were prepared by dissolving the samples in DMSO and kept dry at room temperature. The purity of the overnight cultures was checked after an incubation period of 8 h. After 8 h, the older micro-organism species inoculums containing approximately $10^4$–$10^6$ colony-forming units per cm$^3$ were used in these analyses. All the analyses were made in three replicates for each and the detailed procedure for measuring the zone of inhibition values (in mm) as described earlier [16, 17]. The zone of inhibition values were compared with tetracycline (for antibacterial) and nystatin (for antifungal) control drugs ($3 \times 10^{-3}$ mol), respectively. The zone of inhibition is given as the average of three independent determinations.

### 2.3.2. **Antioxidant activity**. *In vitro* antioxidant activities of free 2-aminobenzamide (2AB : L) and its complexes have been investigated by DPPH (2,2-diphenyl-1-picrylhydrazyl) free radical scavenging model according to the Blois method [26]. The stock solutions (250 μmol) for free 2AB(L) and its complexes in DMSO (20 mL) were prepared.

Different concentrations (10, 20, 30, 40, and 50 μmol) from the stock solutions were made by dilution. One milliliter samples of each solution of different concentrations were taken in different test tubes and 0.1 mmol ethanolic DPPH solution (4 mL) was added and the reaction mixture was shook vigorously for 2–3 min. Then, each tube was incubated in the dark room for 30 min at room temperature. A blank DPPH solution (without sample) was used for the baseline correction because the odd electron in the DPPH-free radical gives a strong absorption maximum ($\lambda_{max}$) at 517 nm (purple color with $\varepsilon = 8.32 \times 10^3$ mol$^{-1}$ cm$^{-1}$) using a Hitachi U-2000 double-beam spectrophotometer. After incubation, the absorbance values of each solution were measured at 517 nm and a change (decrease) in the absorbance ($\lambda_{max}$) values indicated that the complexes have significant free radical scavenging activity. Ascorbic acid was used as the reference or positive control and the free radical scavenging activity (in %) was calculated using this formula:

$$\text{Radical scavenging activity} (\%) = \left[ \frac{(A_{control} - A_{sample})}{A_{control}} \right] \times 100$$

where $A_{control}$ is the absorbance of the control without the ligand or complexes and $A_{sample}$ is the absorbance of the ligand or complexes. Each analysis was made in triplicate and the mean results were compared with the control.

### 2.4. Interaction between heteroligand MLB complexes with DNA

The DNA experiment was carried out in Tris buffer (5 mmol Tris–HCl, 5 mmol NaCl, pH 7.2) with the complexes in DMSO. The CT-DNA concentration per nucleotide $[C(p)]$ was determined by electronic absorption spectroscopy using the molar absorption coefficient ($\varepsilon = 6600$ mol$^{-1}$ cm$^{-1}$) value at 260 nm [27]. The purity of the CT-DNA was checked by its absorbance values at 260 nm, 280 nm and the ratio $A_{260}/A_{280}$ was found to be 1.87, indicating that CT-DNA was sufficiently free from protein contamination [28]. The stock solution (in 1 : 100 dilutions at 4 °C) was not used after four days. Doubly distilled, $CO_2$-free water was used to prepare the buffer and other required solutions.

**2.4.1. Binding studies**. The interaction between the MLB complexes and DNA were studied by electronic absorption and fluorescence techniques.

2.4.1.1. *Electronic absorption study.* The electronic absorption spectra of the synthesized heteroligand complexes ($1 \times 10^{-5}$ M) were recorded in the presence and absence of CT-DNA in DMSO solution in Tris buffer. The binding experiments were done by varying the concentration of CT-DNA concentration (0–100 μmol) while keeping the complexes' concentration as constant. After successive addition of CT-DNA to the complex solution, the resulting mixture was shaken then allowed to equilibrate (5–10 min) at room temperature and the absorption values were recorded. The DNA-binding titration processes were repeated until there was no change in the spectra, which indicated binding saturation was attained. To know quantitatively, the binding strength (intrinsic binding constant: $K_b$) of the complexes was evaluated with increasing CT-DNA concentration using the function equation [29] as follows:

$$\frac{[\text{DNA}]}{(\varepsilon_a - \varepsilon_f)} = \frac{[\text{DNA}]}{(\varepsilon_b - \varepsilon_f)} + \frac{1}{K_b(\varepsilon_b - \varepsilon_f)}$$

where $\varepsilon_f$, $\varepsilon_b$, and $\varepsilon_a$ are the molar extinction coefficients of the free complex in solution, completely bound form of the complex to CT-DNA, and complex bound to CT-DNA at a definite concentration, respectively. The observed absorption data were then fitted into the above equation, i.e. a plot of $[\text{DNA}]/(\varepsilon_b - \varepsilon_f)$ *versus* $[\text{DNA}]$ gave a straight line with a slope of $1/(\varepsilon_b - \varepsilon_f)$ and a *y*-intercept of $1/K_b(\varepsilon_b - \varepsilon_f)$. The $K_b$ value was determined from the ratio of the slope to *y*-intercept [30].

2.4.1.2. *Fluorescence study*. The binding affinity of the heteroligand complexes to CT-DNA was also determined by a fluorescent spectral technique using ethidium bromide (EB) bound CT-DNA solution in Tris buffer (5 mmol Tris–HCl, 5 mmol NaCl, pH 7.2) medium. In a typical fluorescence binding experiment, the fixed concentration of the heteroligand complexes ($1 \times 10^{-5}$ mol) was titrated with the increasing amounts of CT-DNA (0–100 μmol) in EB ($1 \times 10^{-5}$ mol) solution [31]. In the presence of CT-DNA, EB emits an intense fluorescence intensity which is due to its strong intercalative binding to DNA, whereas the addition of complex to CT-DNA shows a decrease in the emission intensity of EB. The fluorescence spectra were recorded at room temperature with excitation intensity ($\lambda_{ex}$) at 546 nm and emission intensity ($\lambda_{em}$) at 602 nm. A control experiment was also done with the EB solution (without CT-DNA) for the baseline correction of the fluorescence intensity.

**2.4.2. Oxidative DNA cleavage study**. The oxidative DNA cleavage activities of free 2-aminobenzamide (2AB) and its Cu(II) complexes (**2a**–**2d**) with calf thymus DNA (CT-DNA) were monitored by agarose gel electrophoresis. The experiments were performed under aerobic conditions with $H_2O_2$ as oxidant by incubation at 37 °C for 2 h as follows: CT-DNA, 30 μmol, 50 μmol of each heteroligand complex, 50 μmol of $H_2O_2$ in 50 mmol Tris–HCl buffer (pH 7.2) containing 50 mmol NaCl solution. After incubation, 1 μL of loading buffer (bromophenol blue in $H_2O$) was added to each tube and the samples were loaded on 1% agarose gel. The samples were examined through electrophoresis at a constant voltage (50 V) for 2 h in Tris–acetic acid–EDTA buffer (40 mmol Tris–acetate, 1 mmol EDTA, pH 8.0). After electrophoresis, the gel was stained for 30 min by immersing it in 1 μg cm$^{-3}$ EB solution. The DNA cleavage was visualized by viewing the gel under ultraviolet (UV) light and photographed.

**2.5.** *pH-metric and spectrophotometric measurements*

The pH-metric titrations were carried out using a digital pH meter (Elico LI Systems 127) with a combined glass and calomel electrode (accuracy of ±0.01 pH unit) in 50% (v/v) water–ethanol mixture at 37 °C under an $N_2$ atmosphere and the instrument was calibrated periodically using standard buffer solutions [32]. The temperature of each solutions were maintained using a Toshniwal GL 15.01 thermostat bath with an accuracy of ±0.1 °C. The ionic strength ($I = 0.15$ mol dm$^{-3}$) of the entire title complexes was maintained by addition of sodium perchlorate as supporting electrolyte. The titrations were carried out on aliquots (50 mL) of solution containing low concentrations of corresponding metal(II) perchlorate

$(3 \times 10^{-3}$ mol), 2AB(L) and imidazole ligands (B) in $1:1:1$ and $1:1:2$ ratios with known volume of standard $CO_2$-free sodium hydroxide solution. All the calculations involved in the potentiometric study within the pH range of 2.5–9.0 (50–70 observations; volume of base/pH) are given in table S1 (Supplementary data file). The obtained pH-metric data were computed with the aid of SCOGS computer program [33]. All the calculations have been restricted to complexes below pH 9.0 since the region above this pH is complicated due to hydrolysis. By increasing the pH level (>9.0), the titled complexes undergo hydroxylation and form $[M(OH)_2]$ as precipitate and thus, no calculations have been implemented beyond this point. Therefore, a critical evaluation of the hydroxo complexes will not be performed in the present estimation. Oxygen-free $N_2$ gas was bubbled through the solution before and during titrations. The pH-meter readings in 50% (v/v) water–ethanol medium were corrected by the Van Uitert and Haas relation [34]. The ionic product of water $(K_W)$ was calculated in 50% (v/v) water–ethanol medium based on the measurement of $[H^+]$ and $[OH^-]$ at constant $I = 0.15$ mol $dm^{-3}$ $NaClO_4$ medium. The obtained $K_W$ (14.39 $\pm$ 0.02 at 37 °C) value of the complex is in agreement with the already reported data [35]. The protonation and primary stability constant of ligands (B) were redetermined under the same experimental conditions. Multiple titrations were carried out for each complex and the formation of various species distribution curves of the metal speciation in solution were calculated by HySS program [36]. Under the same experimental condition, the maximum concentration of the complex species at different pH (ca. 2.0–9.0) intervals (from the supporting of pH-metric studies) were freshly prepared and their electronic spectra were measured on a Hitachi U-2000 double-beam spectrophotometer (cell length, 1 cm) from 200 to 1100 nm at 37 °C.

## 3. Results and discussion

### 3.1. *Solid-state study of the MLB complexes*

**3.1.1. Analytical, FAB-MS, and conductivity measurements**. All the synthesized heteroligand MLB complexes have characteristic color with good yield, stable in the absence of air and moisture, and non-hygroscopic in nature. The analytical and various physicochemical properties of the complexes are summarized in table 1. From the analytical data, the synthesized complexes agree well with the calculated values and confirmed $1:1:1$ (metal : 2-aminobenzamide : imidazole) molar ratio. The conductance $(\Lambda_m)$ of the title complexes was measured in DMSO (~$10^{-3}$ mol) solution at room temperature and the observed low molar conductance (5.5–10.6 mho $cm^2$ $mol^{-1}$) values suggest that all the complexes are non-electrolytes [37]. The FAB-MS of Ni(II)/Cu(II)/Zn(II)–2AB(L)–him(B) complexes (**1a**, **2a** and **3a**) exhibits a molecular ion $(M^+)$ peak at $m/z$ values 400 (33%), 404 (16%), and 405 (18%), respectively. The FAB-MS of Ni(II) and Cu(II)–2AB(L)–him (B) complexes (**1a** and **2a**) is given in figures S1 and S2 (Supplementary data file) which suggests that the complexes are monomeric and confirming the stoichiometry of the metal to ligands ratio is $1:1:1$ in all the complexes.

**3.1.2. Vibrational study**. The vibrational spectra help to investigate the mode of coordination between the free ligands (L and B) with M(II) ions by comparing the spectral data of

Table 1. Analytical and various physicochemical properties of the heteroligand complexes.

| Complex | Color | Empirical formula | Yield (%) | Elemental analysis, found (Calcd) (%) | | | | $\Lambda_m{}^a$ ($\Omega^{-1}$ cm$^2$ mol$^{-1}$) |
| --- | --- | --- | --- | --- | --- | --- | --- | --- |
| | | | | M | C | H | N | |
| Ni(II)–2AB(L)–him(B) (**1a**) | Pale green | NiC$_{14}$H$_{18}$O$_5$N$_4$·H$_2$O | 72 | 14.57 (14.71) | 42.01 (42.14) | 4.92 (5.05) | 14.61 (14.71) | 6.2 |
| Ni(II)–2AB(L)–bim(B) (**1b**) | Pale green | NiC$_{18}$H$_{20}$O$_5$N$_4$·H$_2$O | 65 | 12.92 (13.07) | 48.06 (48.14) | 4.81 (4.94) | 12.22 (12.48) | 8.1 |
| Ni(II)–2AB(L)–hist(B) (**1c**) | Green | NiC$_{16}$H$_{23}$O$_5$N$_5$ | 70 | 13.77 (13.84) | 45.19 (45.32) | 5.39 (5.47) | 16.44 (16.51) | 8.9 |
| Ni(II)–2AB(L)–his(B) (**1d**) | Green | NiC$_{15}$H$_{19}$O$_5$N$_5$ | 74 | 14.22 (14.38) | 43.94 (44.15) | 4.61 (4.69) | 17.06 (17.16) | 7.2 |
| Cu(II)–2AB(L)–him(B) (**2a**) | Brown | CuC$_{14}$H$_{18}$O$_5$N$_4$·H$_2$O | 68 | 15.62 (15.73) | 41.56 (41.63) | 4.88 (4.99) | 13.94 (14.04) | 6.8 |
| Cu(II)–AB(L)–bim(B) (**2b**) | Brown | CuC$_{18}$H$_{20}$O$_5$N$_4$·H$_2$O | 64 | 13.89 (14.00) | 47.56 (47.63) | 4.76 (4.88) | 12.23 (12.34) | 5.5 |
| Cu(II)–2AB(L)–hist(B) (**2c**) | Dark brown | CuC$_{16}$H$_{23}$O$_5$N$_5$ | 72 | 14.67 (14.81) | 44.69 (44.80) | 5.28 (5.40) | 16.25 (16.33) | 5.9 |
| Cu(II)–2AB(L)–his(B) (**2d**) | Dark brown | CuC$_{15}$H$_{19}$O$_5$N$_5$ | 75 | 15.32 (15.39) | 43.48 (43.63) | 4.59 (4.64) | 16.78 (16.96) | 8.3 |
| Zn(II)–2AB(L)–him(B) (**3a**) | White | ZnC$_{14}$H$_{18}$O$_5$N$_4$·H$_2$O | 66 | 16.01 (16.12) | 41.32 (41.44) | 4.86 (4.97) | 13.68 (13.81) | 9.3 |
| Zn(II)–2AB(L)–bim(B) (**3b**) | White | ZnC$_{18}$H$_{20}$O$_5$N$_4$·H$_2$O | 60 | 14.21 (14.35) | 47.28 (47.43) | 4.71 (4.87) | 12.11 (12.29) | 8.4 |
| Zn(II)–2AB(L)–hist(B) (**3c**) | White | ZnC$_{16}$H$_{25}$O$_5$N$_5$ | 67 | 15.02 (15.11) | 44.21 (44.40) | 5.62 (5.82) | 16.02 (16.18) | 7.9 |
| Zn(II)–2AB(L)–his(B) (**3d**) | White | ZnC$_{15}$H$_{19}$O$_5$N$_5$ | 70 | 15.61 (15.77) | 43.23 (43.44) | 4.50 (4.62) | 16.78 (16.89) | 10.6 |

$^a$Solvent medium for the conductance ($\Lambda_m$) measurements was DMSO.

Table 2.　IR spectral data of primary ligand(L), secondary ligands(B), and its heteroligand complexes (in cm$^{-1}$).

| Sl. No. | Complex | $\nu$(M–O) | $\nu$(M–N) | $\nu_{C=O}$(CONH$_2$) | $\nu_{NH}$(CONH$_2$) | $\nu_{NH}$(NH$_2$) | $\nu_{ring}$(NH) | $\nu$(C=N) | $\nu$(H$_2$O) | $\nu$(COO$^-$)$_s$ | $\nu$(COO$^-$)$_{as}$ |
|---|---|---|---|---|---|---|---|---|---|---|---|
| 1. | 2-Aminobenzamide(L) | – | – | 1656 | 3182 | 3410 | – | – | – | – | – |
| 2. | Imidazole(B) | – | – | – | – | – | 3145 | 1621 | – | – | – |
| 3. | Benzimidazole(B) | – | – | – | – | – | 3144 | 1609 | – | – | – |
| 4. | Histamine(B) | – | – | – | – | 3325 | 3146 | 1628 | – | – | – |
| 5. | L-Histidine(B) | – | – | – | – | 3330 | 3147 | 1634 | – | 1589 | 1367 |
| 6. | Ni(II)–2AB(L)–him(B) (**1a**) | 419 | 576 | 1670 | 3180 | 3402,3315 | 3144 | 1612 | 3380,844,711 | 1572 | 1369 |
| 7. | Ni(II)–2AB(L)–bim(B) (**1b**) | 416 | 573 | 1666 | 3183 | 3401,3312 | 3145 | 1601 | 3384,825,708 | 1588 | 1358 |
| 8. | Ni(II)–2AB(L)–hist(B) (**1c**) | 433 | 579 | 1669 | 3182 | 3396,3317 | 3144 | 1617 | – | 1601 | 1399 |
| 9. | Ni(II)–2AB(L)–his(B) (**1d**) | 428 | 586 | 1671 | 3183 | 3398,3307 | 3146 | 1619 | – | 1579 | 1356 |
| 10. | Cu(II)–2AB(L)–him(B) (**2a**) | 428 | 576 | 1671 | 3182 | 3402,3310 | 3145 | 1616 | 3388,834,721 | 1575 | 1384 |
| 11. | Cu(II)–AB(L)–bim(B) (**2b**) | 430 | 580 | 1661 | 3183 | 3397,3313 | 3145 | 1604 | 3450,858,724 | 1596 | 1365 |
| 12. | Cu(II)–2AB(L)–hist(B) (**2c**) | 436 | 590 | 1667 | 3182 | 3399,3315 | 3144 | 1618 | – | 1621 | 1394 |
| 13. | Cu(II)–2AB(L)–his(B) (**2d**) | 438 | 596 | 1669 | 3180 | 3401,3308 | 3145 | 1622 | – | 1581 | 1354 |
| 14. | Zn(II)–2AB(L)–him(B) (**3a**) | 415 | 566 | 1664 | 3182 | 3396,3312 | 3146 | 1617 | 3402,822,710 | 1605 | 1389 |
| 15. | Zn(II)–2AB(L)–bim(B) (**3b**) | 414 | 569 | 1662 | 3181 | 3398,3311 | 3144 | 1603 | 3394,849,719 | 1598 | 1379 |
| 16. | Zn(II)–2AB(L)–hist(B) (**3c**) | 429 | 577 | 1668 | 3183 | 3395,3316 | 3145 | 1614 | – | 1610 | 1376 |
| 17. | Zn(II)–2AB(L)–his(B) (**3d**) | 432 | 584 | 1670 | 3182 | 3404,3314 | 3146 | 1624 | – | 1577 | 1359 |

the free ligands with the spectra of the complexes. The characteristic IR spectral bands of the complexes (KBr pellets, cm$^{-1}$) are listed in table 2. All the complexes show two bands at 1572–1621 and 1356–1399 cm$^{-1}$, ascribed as asymmetric and symmetric vibration of the coordinated acetate [38]. The magnitude of $\Delta v$ of 215–223 cm$^{-1}$ suggests unidentate coordination of acetate. The presence of coordinated water in M(II)–2AB(L)–him/bim(B) complexes is indicated by a broad band from 3380 to 3450 cm$^{-1}$ and two weaker bands at 822–858 cm$^{-1}$ and 708–724 cm$^{-1}$ due to $v$(OH) rocking and wagging of coordinated water, respectively, in these complexes [38–40]. Free 2AB(L) shows peaks at 3410, 3182, and 1656 cm$^{-1}$ due to vibrations of N-amino, N-amido, and O-carbonyl amide groups, respectively. On complexation, a broad band at 3396–3402 cm$^{-1}$ indicates coordination of N-amino in the complexes. The unchanged peak at 3182 cm$^{-1}$ in the complex spectra indicates non-involvement of $v_{NH}(CONH_2)$ of N-amido group in coordination. The band at 1656 cm$^{-1}$ is shifted to higher frequencies (1661–1670 cm$^{-1}$) due to O-carbonyl amide involved in complexation [16, 17, 41]. This implies that 2-aminobenzamide(L) binds with M(II) through N-amino and O-amido groups [38, 41] to form stable six-membered chelates. This is further supported by bands in the far infrared region, 414–438 cm$^{-1}$, corresponding to (M–O) and 566–596 cm$^{-1}$ to (M–N) bond stretches, respectively [38, 40]. The $v$(M–O) and $v$(M–N) values follow Irving–William order of stability as: Cu(II) > Ni(II) > Zn(II) and also comparable with the crystal field stabilization energies. In M(II)–2AB(L)–him/bim/hist (B) complexes, the unchanged band at 3144–3147 cm$^{-1}$ assigned to $v$(N–H) stretch of the imidazole ring indicates non-involvement of the imidazole ring (–NH–) in coordination [38–40]. The bands at 1634–1609 cm$^{-1}$ assigned to imidazole ring $v$(C=N) stretch shifted to lower frequency by 8–15 cm$^{-1}$, indicating participation of the imidazole ring nitrogen in chelation in M(II)–2AB(L)–him/bim/hist/his(B) complexes. Also, M(II)–2AB(L)–hist/his(B) complexes show a group of bands from 3325 to 3035 cm$^{-1}$ in the spectra, which can be attributed to the stretching of the coordinated $NH_2$ group [38]. The asymmetric and symmetric stretching vibrations of the carboxylate in free his(B) at 1589 and 1367 cm$^{-1}$ are shifted lower by 8–12 cm$^{-1}$ in M(II)–2AB(L)–his(B) complexes, suggesting that the deprotonated O-carboxylato group of his(B) chelates with M(II) ions.

**3.1.3. Magnetic measurements and electronic absorption spectra.** The magnetic moment ($\mu_{eff}$ = 3.14–3.21 BM) values of heteroligand NiLB complexes (**1a**–**1d**) correspond to two unpaired electrons per Ni(II) ion with $D_{4h}$ symmetry having octahedral geometry [23, 42]. These observed values also support the absence of any metal–metal interaction in the solid phase, i.e. ruled out bimetallic complexes. The magnetic measurements of Cu(II) complexes (**2a**–**2d**) show 1.82–1.89 BM, which is slightly higher than the spin-only value 1.73 BM expected for one unpaired electron. The observed value offers possibility of a distorted octahedral geometry [23, 42]. In order to determine the stereochemistry around M(II) ions, the electronic absorption spectra of M(II)–2AB(L)–him/bim/hist/his(B) complexes (1 × 10$^{-3}$ M) were recorded in DMSO medium at ambient temperature from 200 to 1100 nm. Absorption regions ($\lambda_{max}$), band assignments, proposed geometry, ligand field parameters, and magnetic moment values of the complexes are given in table 3. In Ni(II)–2AB(L)–him/bim/hist/his(B) complexes (**1a**–**1d**), three absorption bands occur at 10,322–10,515 ($\varepsilon$ = 76–88 dm$^3$ mol$^{-1}$ cm$^{-1}$), 16,892–17,353 ($\varepsilon$ = 112–132 dm$^3$ mol$^{-1}$ cm$^{-1}$), and 24,876–26,247 ($\varepsilon$ = 252–264 dm$^3$ mol$^{-1}$ cm$^{-1}$) cm$^{-1}$ corresponding to $^3A_{2g}$ (F) → $^3T_{2g}$ (F), $^3A_{2g}$ (F) → $^3T_{1g}$ (F), and $^3A_{2g}$ (F) → $^3T_{1g}$ (P) transitions, respectively, with an octahedral geometry with $^3A_{2g}$ as ground state [43]. Water or acetate molecules on the *z*-axis of the

Table 3. Electronic absorption spectral data, ligand field parameters, and magnetic measurement values of M(II)–2AB–him, bim, hist, and his complexes (in DMSO) at 37 °C.

| Complex | λmax (cm⁻¹) ε (dm³ mol⁻¹ cm⁻¹) Solution state | Solid state | Band assignments | Geometry | μeff (BM) | Lunde's factor (g) | Ligand field parameter Dq (cm⁻¹) | B (cm⁻¹) | β | β (%) | LFSE (kJ mol⁻¹) | ν₂/ν₁ |
|---|---|---|---|---|---|---|---|---|---|---|---|---|
| Complex (1a) | 10,980 (65)<br>16,565 (112)<br>23,546 (235) | 10,438 (85)<br>17,190 (120)<br>25,330 (252) | ³A₂g(F) → ³T₂g(F)<br>³A₂g(F) → ³T₁g(F)<br>³A₂g(F) → ³T₁g(P) | Octahedral | 3.14 | 2.278 (2.250 for hexaaquo Ni(II) complexes) | 1044 | 747.07 (1030 for free ion) | 0.73 | 27.47 | 149.94 | 1.65 |
| Complex (1b) | 10,864 (60)<br>16,153 (120)<br>22,455 (248) | 10,350 (80)<br>16,935 (112)<br>25,671 (264) | ³A₂g(F) → ³T₂g(F)<br>³A₂g(F) → ³T₁g(F)<br>³A₂g(F) → ³T₁g(P) | Octahedral | 2.98 | 2.272 | 1035 | 770.40 | 0.75 | 25.20 | 148.67 | 1.64 |
| Complex (1c) | 11,080 (62)<br>17,298 (110)<br>25,650 (232) | 10,322 (76)<br>16,892 (128)<br>24,876 (254) | ³A₂g(F) → ³T₂g(F)<br>³A₂g(F) → ³T₁g(F)<br>³A₂g(F) → ³T₁g(P) | Octahedral | 3.08 | 2.281 | 1032 | 720.13 | 0.70 | 30.08 | 148.27 | 1.64 |
| Complex (1d) | 11,135 (70)<br>18,920 (128)<br>26,840 (242) | 10,515 (88)<br>17,353 (132)<br>26,247 (258)<br>35,714 (780) | ³A₂g(F) → ³T₂g(F)<br>³A₂g(F) → ³T₁g(F)<br>³A₂g(F) → ³T₁g(P)<br>LMCT | Octahedral | 3.21 | 2.288 | 1052 | 803.67 | 0.78 | 21.97 | 151.04 | 1.65 |
| Complex (2a) | 14,677 (140) | 14,871 (147) | ²Eg(D) → ²T₂g(D) | Distorted octahedral | 1.85 | – | – | 828 (for free ion) | – | – | – | – |
| Complex (2b) | 14,246 (148) | 14,326 (152) | ²Eg(D) → ²T₂g(D) | Distorted octahedral | 1.82 | – | – | – | – | – | – | – |
| Complex (2c) | 14,359 (153) | 14,577 (141) | ²Eg(D) → ²T₂g(D) | Distorted octahedral | 1.86 | – | – | – | – | – | – | – |
| Complex (2d) | 14,781 (165) | 14,759 (146) | ²Eg(D) → ²T₂g(D) | Distorted octahedral | 1.89 | – | – | – | – | – | – | – |
| Complex (3a) | – | 26,338 (180) | LMCT | Octahedral | Dia. | – | – | – | – | – | – | – |
| Complex (3b) | – | 26,247 (184) | LMCT | Octahedral | Dia. | – | – | – | – | – | – | – |
| Complex (3c) | – | 26,455 (172) | LMCT | Octahedral | Dia. | – | – | – | – | – | – | – |
| Complex (3d) | – | 26,507 (179) | LMCT | Octahedral | Dia. | – | – | – | – | – | – | – |

Cartesian coordinate make them six-coordinate octahedral. Absence of any band below 10,000 cm$^{-1}$ ruled out the possibility of a tetrahedral environment. The observed $v_2/v_1$ ratios are expected for distorted octahedral environment around Ni(II). Furthermore, the calculated $B$ value is less than free Ni(II) ion ($B^\mathrm{o} = 1030$ cm$^{-1}$), $\beta$ (0.70–0.78), and % $\beta^\circ$ (22–30) values support the covalent character of the Ni(II) complexes with $D_{4h}$ symmetry around the Ni(II) ion [44, 45]. Cu(II)–2AB(L)–him/bim/hist/his(B) complexes (**2a**–**2d**) with moderate Jahn–Teller distortion exhibit only one broad band with maximum at 13,555–15,680 cm$^{-1}$ centered at 14,871, 14,326, 14,577, and 14,759 cm$^{-1}$ ($\varepsilon = 141$–152 dm$^3$ mol$^{-1}$ cm$^{-1}$) corresponding to $^2\mathrm{E_g}$ (D) $\rightarrow$ $^2\mathrm{T_{2g}}$ (D) transition, respectively, in distorted octahedral environment [43] with the unpaired electron predominantly in $d_{x_2-y_2}$ ground state. Furthermore, the observed magnetic measurement values are in agreement for the above-assigned geometry. The Zn(II) ion is diamagnetic and does not show any d–d transitions. However, **3a**–**3d** show only one broad band in the UV region at 26,338, 26,247, 26,455, and 26,507 cm$^{-1}$ ($\varepsilon = 172$–184 dm$^3$ mol$^{-1}$ cm$^{-1}$) which may be due to L $\rightarrow$ M charge transfer (LMCT) transition with six-coordinate octahedral environment around Zn(II) [43].

**3.1.4. EPR spectra of heteroligand Cu(II) complexes**. The X-band EPR spectra of polycrystalline Cu(II)–2AB(L)–him/bim/hist/his(B) complexes (**2a**–**2d**) in DMSO were recorded at ambient (300 K) and liquid nitrogen (77 K) temperatures; the EPR spectrum of Cu(II)–2AB(L)–his(B) is shown in figure 2. At 300 K, EPR spectra of Cu(II) complexes exhibit one intense absorption band in the high-field region and this is isotropic due to the tumbling motion of the molecules, i.e. the magnetic coupling between the unpaired electron with effective Cu nuclei ($I = 3/2$). In the case of frozen solution (77 K), EPR spectra show four well-resolved peaks of low intensities in low-field region and one intense peak in high-field region with anisotropic pattern which indicates the absence of binuclear, i.e. monomeric nature of Cu(II) complexes [46, 47]. This is further supported by the observed $\mu_{\mathrm{eff}}$ values of the CuLB complexes. The spectra of Cu(II) complexes are axially symmetric with g-tensor values, $g_\parallel$ (2.18–2.29) $> g_\perp$ (2.01–2.03) $> g_\mathrm{e}$ (2.0023) and these g-tensor values clearly indicate that the unpaired electron is localized in $d_{x_2-y_2}$ orbital [43, 46] of Cu(II) ion with 3d$^9$ configuration. The observed g-tensor values are less than 2.3 which indicate covalent Cu(II)–Ligand(s) bond and the calculated g average ($g_{\mathrm{avg}} = 2.07$–2.11) values of Cu(II) complexes deviate from free electron ($g_\mathrm{e} = 2.0023$) value which also supports covalence in Cu(II)–Ligand(s) bonding [47]. The absence of any half-field signal at 1600 $G$ corresponding to $\Delta M_\mathrm{s} = \pm2$ transitions rules out any magnetic exchange, i.e. Cu–Cu interactions in the complexes. The calculated spin Hamiltonian and bonding parameter values of Cu(II) complexes are given in table 4. The observed axial symmetry $G$ values are less than four, which indicate considerable exchange interaction present in the solid CuLB complexes. Further, the calculated bonding parameter ($\alpha^2 = 0.58$–0.71 and $\beta^2 = 0.76$–0.84) values of Cu(II) complexes (**2a**–**2d**) clearly indicate that $\sigma$-bonding is more covalent than in-plane $\pi$-bonding [48]. From table 4, the $\alpha^2$ and $\beta^2$ values reflect higher covalence of the Cu(II)–ligand(s) bonding in the complexes and these values follow the order his > hist > him > bim, which corresponds to increasing electron density on the coordinating nitrogen. The observed $A_\parallel$ values (121–136 × 10$^{-4}$ cm) are comparable to reported distorted octahedral Cu(II) complexes [16, 46]. The distortion from the plane increases with increasing $g_\parallel$ values and decreasing $A_\parallel$ values. The geometries of the complexes are further studied from the empirical factor ($f$), i.e. $f = \frac{g_\parallel}{A_\parallel}$, an index of tetragonal distortion and the calculated $f$ values for

CuLB complexes are very close to 166–173 cm, indicating a distorted octahedral environment around Cu(II) [16, 46].

**3.1.5. $^1$H NMR spectra**. The $^1$H NMR spectra of diamagnetic ZnLB complexes (**3a–3d**) were recorded in DMSO-d$_6$ with TMS as internal standard ($\delta$, in ppm) at room temperature; the $^1$H NMR spectra of Zn(II)–2AB(L)–him(B) (**3a**) is shown in figure 3. In free 2AB(L), the proton of ring amino (NH$_2$) and amide amino (CONH$_2$) groups appear as singlets at
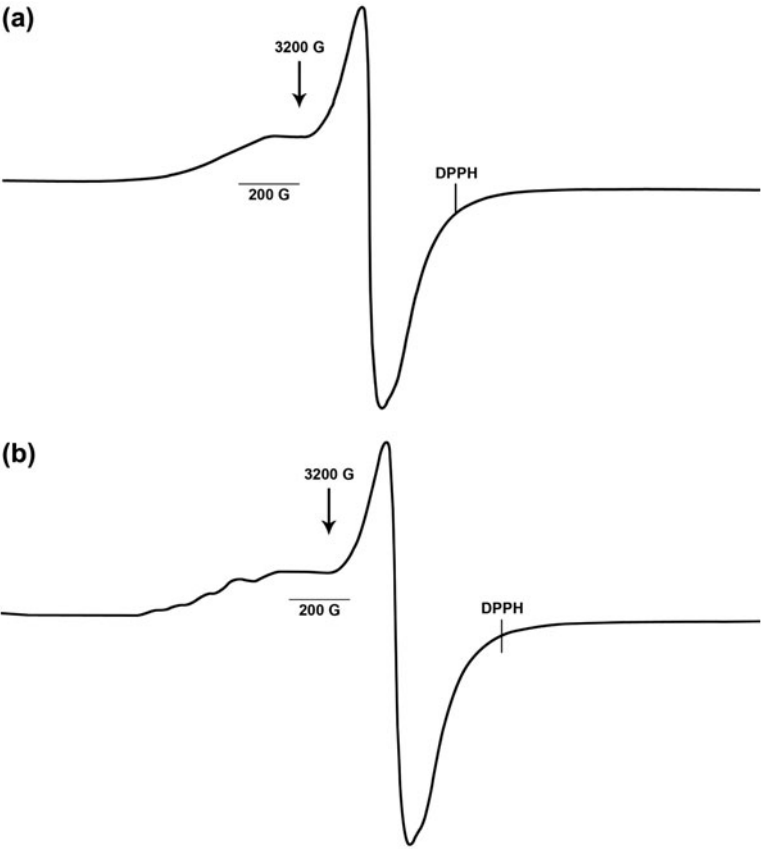


Figure 2.   X-band EPR spectrum of Cu(II)–2AB–his complex (a) at 300 K and (b) 77 K in DMSO medium.

Table 4.   The spin Hamiltonian and bonding parameter values of Cu(II) complexes (**2a–2d**) in DMSO at 300 and 77 K.

| Complex | Hyperfine constant $\times 10^{-4}$ cm$^{-1}$ | | | | | | | | | | |
|---|---|---|---|---|---|---|---|---|---|---|---|
| | $A_\parallel$ | $A_\perp$ | $A_{\text{iso}}$ | $g_\parallel$ | $g_\perp$ | $g_{\text{iso}}$ | $\alpha^2$ | $\beta^2$ | $\alpha$ | $f = \frac{g_\parallel}{A_\parallel}$ | $G$ |
| Complex (**2a**) | 121 | 54 | 77 | 2.25 | 2.02 | 2.12 | 0.63 | 0.78 | 0.88 | 167 | 13.99 |
| Complex (**2b**) | 129 | 49 | 71 | 2.18 | 2.01 | 2.10 | 0.58 | 0.76 | 0.66 | 169 | 23.08 |
| Complex (**2c**) | 136 | 58 | 89 | 2.26 | 2.03 | 2.13 | 0.69 | 0.83 | 0.83 | 166 | 9.30 |
| Complex (**2d**) | 132 | 45 | 68 | 2.29 | 2.03 | 2.11 | 0.71 | 0.84 | 0.91 | 173 | 10.39 |

Figure 3.  $^1$H NMR spectra of Zn(II)–2AB–him complex (**3a**).

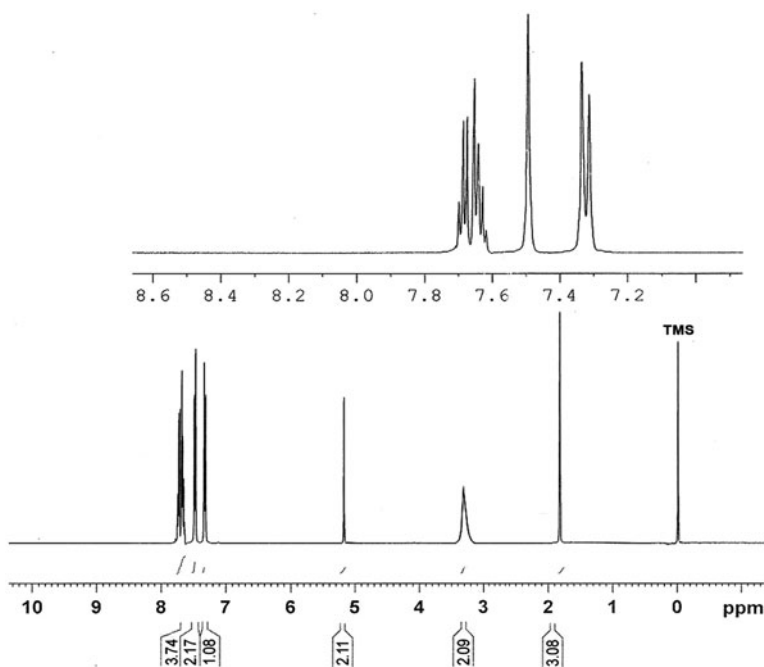5.66 and 7.31 ppm, respectively; upon complexation, the peak at 5.66 ppm shifts to higher field (5.20–5.10), whereas the amine in amide group does not show any change [49]. This indicates that 2AB(L) chelates Zn(II) ion via N-amino and O-amido to form stable metal chelates. All the Zn(II) complexes (**3a**–**3d**) show singlets at 7.50–7.62 ppm due to the imidazole ring (–HC=N–) proton. The rest of the ring proton and the ring (–NH–) protons in him/bim ligands(B) do not have any change in Zn(II)–2AB(L)–him/bim(B) complexes. This indicates that him/bim(B) ligands coordinate to Zn(II) only through imidazole nitrogen. All of the Zn(II) complexes show a peak at 1.80–1.86 ppm with the integrated intensity of 3 (CH$_3$ group), indicating that acetate (OAc) is coordinated with Zn(II). There are new peaks at 3.30–3.78 ppm in Zn(II)–2AB(L)–him/bim(B) complexes, indicating coordinated water molecules are present [49]. Thus, coordinated water and monodentate acetate bind in the inner coordination sphere of the complexes. This is further confirmed from the observed molar conductivity values, i.e. non-electrolytic nature of the complexes. All the protons are in their expected regions [49]. The $\alpha$-proton of free his(B) shows a multiplet at 3.84 ppm, which is shifted to higher value of 4.18 ppm in the Zn(II)–2AB(L)–his(B) complex (**3d**). This shift is larger than that **3c**, indicating that his coordinates to Zn(II) ion through the O-carboxylato, N-amino, and imidazole ring-N atoms, whereas only amino and imidazole ring nitrogens are involved for hist(B) with Zn(II) ion to form octahedral geometry. This study reinforces the conclusions drawn from the IR spectra.

**3.1.6. PXRD study**. PXRD study is used to determine the phase identification of newly synthesized crystalline materials and to measure the sample purity and particle size of the
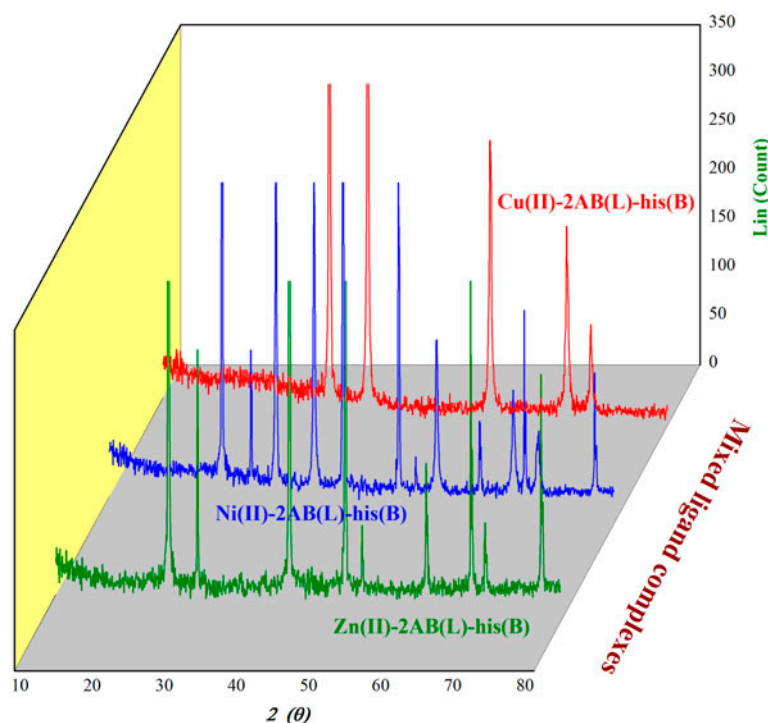
Figure 4.   PXRD patterns of M(II)–2AB–his complexes.

sample materials [50, 51]. In this work, the powder X-ray diffractogram of Ni(II)/Cu(II)/Zn
(II)–2AB(L)–his(B) complexes (**1d**, **2d,** and **3d**) were recorded in the (2 $\theta$) 0–80° range and
the representative diffractograms are given in figure 4. From the XRD patterns, all the com-
plexes show well-resolved sharp peaks with maximum intensities which demonstrate that
the complexes have uniform crystalline state [50]. This behavior is due to the presence of
coordinated water and acetate in the coordination sphere [50–52]. Powder X-ray diffrac-
togram shows a number of weak peaks which imply uniform phase with absence of any
impurities in the complexes [50]. The crystallite sizes (*D*) of the complexes were calculated
from the main XRD peaks using the Debye–Scherrer's equation ($D = 0.9\,\lambda/\beta\cos\theta$). The
observed average crystallite size values were 39.28, 45.61, and 38.89 nm, respectively, for
Ni(II)/Cu(II)/Zn(II)–2AB(L)–his(B) complexes and these values indicate that the complexes
are micro-crystalline with different crystallite size. We were ineffective in growing single
crystals of the complexes.

   The elemental, molar conductivity measurement, and various spectral studies confirmed
that all MLB complexes have distorted octahedral geometry and are monomers. Based on
these conclusions, the structures of the MLB complexes are given in figure 5.

**3.1.7. Biological activity**. *In vitro* biological activity of free 2-aminobenzamide (2AB : L)
and its heteroligand complexes in DMSO were tested against bacterial and fungal organisms
by modified well diffusion method using agar as nutrient. The mean values obtained for
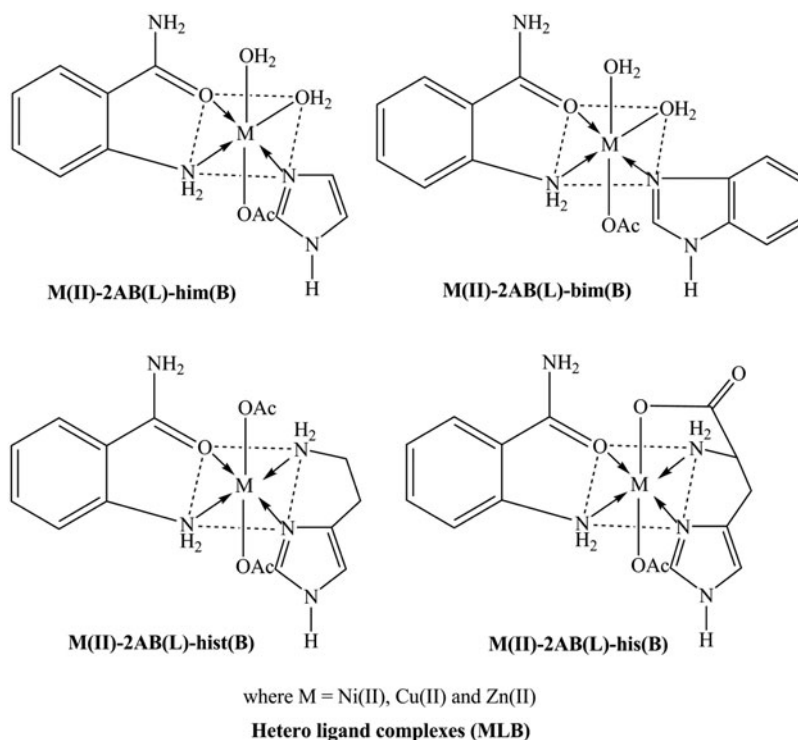
Figure 5. Proposed structure for the MLB complexes.

two holes was used to calculate the zone of inhibition (in mm) and these values were compared with tetracycline (for antibacterial) and nystatin (for antifungal) standard control drugs. The zone of inhibition (in mm) values are given in table 5 and their representative graph is shown in figure 6. All the heteroligand complexes show more biological activities against different micro-organisms than free 2AB(L) ligand. This higher activity depends upon the metal(II) ion, i.e. size, charge distribution, shape, and redox potential of the metal chelates. Also, the chelating properties of organic ligand(s) with specific M(II) ions are used to transport across the membranes or to attach the organic ligand(s) to a specific site as they can hinder the growth of bacteria. This metal chelation effect gives some important properties to the organic molecule(s) that also plays an important role in their microbial activities such as low dissociation constant, special redox potential, electron distribution, and increasing the cell permeability. Moreover, the higher inhibition zone of the MLB complexes can be explained on the basis of Overtone's concept and Tweedy's chelation theory [53, 54]. In the present investigation, the biological activities of free 2AB(L) ligand and its heteroligand MLB complexes against some pathogenic bacterial and fungal organisms show the following order as follows: *Control > MLB complexes (except complex 2d) > 2AB(L)*.

**3.1.8.** *In vitro* **antioxidant activity**. Antioxidant activity of free 2-aminobenzamide(L) ligand and its heteroligand MLB complexes were studied *in vitro* by DPPH free radical scavenging methods at 37 °C and their representative graph is shown in figure 7. Ascorbic

Table 5.  Biological activities of M(II)–2AB–him, bim, hist, and his complexes by well diffusion method at different times (zone formation in mm).

| Complex | Escherichia coli | | | Staphylococcus aureus | | | Staphylococcus saphyphiticus | | | Pseudomonas aeruginosa | | | Aspergillus niger | | | Candida albicans | | | Enterobacter species | | |
|---|---|---|---|---|---|---|---|---|---|---|---|---|---|---|---|---|---|---|---|---|---|
| | 24 | 48 | 72 | 24 | 48 | 72 | 24 | 48 | 72 | 24 | 48 | 72 | 24 | 48 | 72 | 24 | 48 | 72 | 24 | 48 | 72 |
| Control | 22 | 24 | 26 | 28 | 30 | 32 | 27 | 28 | 29 | 32 | 33 | 35 | 32 | 34 | 35 | 24 | 26 | 28 | 33 | 34 | 36 |
| 2AB(L) | – | – | – | 11 | 12 | 13 | 14 | 15 | 17 | – | – | – | 12 | 14 | 16 | 10 | 12 | 15 | – | – | – |
| Complex (**1a**) | 14 | 15 | 17 | 18 | 18 | 19 | – | – | – | 16 | 17 | 18 | 17 | 19 | 20 | – | – | – | 16 | 17 | 17 |
| Complex (**1b**) | 15 | 16 | 16 | – | – | – | 17 | 18 | 19 | – | – | – | 17 | 17 | 18 | 18 | 19 | 20 | 17 | 18 | 19 |
| Complex (**1c**) | 16 | 18 | 20 | 22 | 23 | 24 | – | – | – | 22 | 24 | 25 | 22 | 24 | 25 | 18 | 20 | 21 | – | – | – |
| Complex (**1d**) | – | – | – | 22 | 24 | 25 | – | – | – | 23 | 25 | 26 | – | – | – | 21 | 22 | 23 | 21 | 23 | 26 |
| Complex (**2a**) | 17 | 17 | 19 | 21 | 22 | 22 | 23 | 25 | 26 | – | – | – | 21 | 23 | 23 | – | – | – | 20 | 21 | 21 |
| Complex (**2b**) | 20 | 21 | 21 | 22 | 24 | 25 | 20 | 22 | 23 | 19 | 20 | 21 | 22 | 23 | 23 | 18 | 19 | 19 | – | – | – |
| Complex (**2c**) | 22 | 22 | 23 | – | – | – | – | – | – | 23 | 23 | 24 | 23 | 24 | 25 | 21 | 21 | 23 | – | – | – |
| Complex (**2d**) | 27 | 28 | 29 | 31 | 33 | 36 | 23 | 25 | 26 | 28 | 29 | 31 | – | – | – | 28 | 28 | 30 | 25 | 26 | 28 |
| Complex (**3a**) | 16 | 17 | 18 | 20 | 21 | 21 | – | – | – | 18 | 18 | 20 | 20 | 20 | 21 | 18 | 19 | 21 | 18 | 20 | 22 |
| Complex (**3b**) | 16 | 17 | 18 | 20 | 21 | 21 | 20 | 21 | 22 | 18 | 20 | 20 | – | – | – | 18 | 19 | 19 | – | – | – |
| Complex (**3c**) | – | – | – | 23 | 23 | 24 | 26 | 26 | 27 | 20 | 22 | 23 | 23 | 25 | 26 | 22 | 23 | 25 | 21 | 23 | 24 |
| Complex (**3d**) | 20 | 22 | 24 | 25 | 26 | 28 | 26 | 28 | 29 | – | – | – | – | – | – | – | – | – | – | – | – |

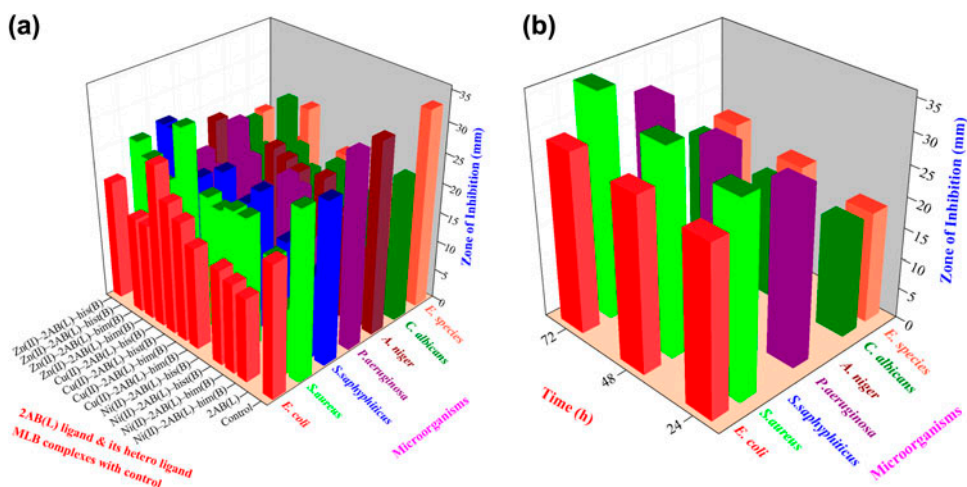Note: (–) = Less active, error limit: ±2–3%.

Figure 6. Biological activities of (a) 2AB and MLB complexes with control at 24 h and (b) heteroligand Cu (II)–2AB–his complex at 24, 48 and 72 h with different micro-organisms by well diffusion method (zone of inhibition in mm).
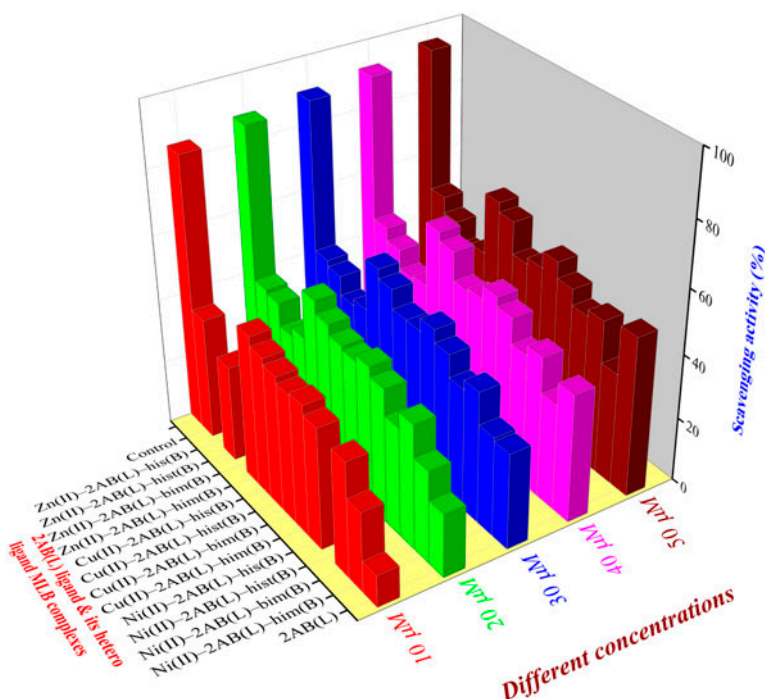


Figure 7. *In vitro* antioxidant activities of free 2AB and MLB complexes with control by DPPH free radical scavenging assay method at different concentrations (10–50 μM).

Table 6.  *In vitro* antioxidant activities of 2-aminobenzamide(L) and its hetero- ligand MLB complexes by DPPH free radical scavenging assay at different concentrations (10–50 μM) at room temperature.

| Complex | Scavenging activity (%) at different concentrations ± SD | | | | |
|---|---|---|---|---|---|
| | 10 μM | 20 μM | 30 μM | 40 μM | 50 μM |
| Control | 85 ± 0.17 | 88 ± 0.18 | 90 ± 0.20 | 92 ± 0.20 | 95 ± 0.21 |
| 2AB(L) | 25 ± 0.18 | 29 ± 0.21 | 31 ± 0.23 | 33 ± 0.25 | 35 ± 0.23 |
| Complex (1a) | 36 ± 0.22 | 39 ± 0.24 | 41 ± 0.26 | 44 ± 0.30 | 48 ± 0.34 |
| Complex (1b) | – | 34 ± 0.21 | 38 ± 0.24 | 41 ± 0.28 | 46 ± 0.31 |
| Complex (1c) | 38 ± 0.24 | 42 ± 0.27 | 45 ± 0.31 | 49 ± 0.34 | 51 ± 0.37 |
| Complex (1d) | 41 ± 0.20 | 45 ± 0.25 | 49 ± 0.27 | 52 ± 0.32 | 56 ± 0.35 |
| Complex (2a) | 40 ± 0.33 | 43 ± 0.35 | 45 ± 0.37 | 48 ± 0.39 | 51 ± 0.43 |
| Complex (2b) | 42 ± 0.29 | 44 ± 0.32 | 45 ± 0.31 | 47 ± 0.29 | 49 ± 0.34 |
| Complex (2c) | 44 ± 0.34 | 47 ± 0.29 | 51 ± 0.33 | 56 ± 0.38 | 59 ± 0.41 |
| Complex (2d) | 47 ± 0.33 | 51 ± 0.34 | 54 ± 0.31 | 59 ± 0.36 | 62 ± 0.38 |
| Complex (3a) | – | 36 ± 0.19 | 38 ± 0.23 | 39 ± 0.27 | 43 ± 0.30 |
| Complex (3b) | 30 ± 0.24 | 33 ± 0.27 | 36 ± 0.31 | 38 ± 0.34 | 40 ± 0.37 |
| Complex (3c) | – | 40 ± 0.29 | 42 ± 0.32 | 44 ± 0.31 | 47 ± 0.34 |
| Complex (3d) | 38 ± 0.26 | 41 ± 0.31 | 44 ± 0.33 | 48 ± 0.37 | 52 ± 0.35 |

Notes: SD : Standard deviation (average of three replicates) and (–) denotes less activity.

acid was used as the reference or positive control. All the analyses were done in three replicates and their average antioxidant activities are shown in table 6. DPPH is a stable free radical that is often used for finding the radical scavenging activity in chemical analysis [55–57]. Reduction capability of DPPH radical was determined by decrease in its absorbance at 517 nm (blank) which can be induced by the antioxidant. From the results, MLB complexes have higher activities than free 2AB(L) ligand but lower than control due to the presence of positively charged M(II) ions which favors the release of hydrogen to reduce the DPPH radical. The percentage of free radical scavenging activity for the heteroligand complexes follow the order *Control* >> *Cu(II)* > *Ni(II)* > *Zn(II)* > *2AB(L)*. From the above results, it clearly indicates that the antioxidant activities of free 2AB(L) is very low when compared to that of its heteroligand complexes, due to the chelation effect of the organic ligand moieties with M(II) ions. Also, the obtained free radical scavenging activity values (51, 49, 59, and 62% at 50 μM) of **2a**–**2d** are consistent with similar mononuclear Cu(II) $[C_{38}H_{28}CuN_2O_2]$ complex [19], which might be due to conjugation in the ligand moieties and their coplanarity. The heteroligand Cu(II) complexes (**2a**–**2d**) showed significantly stronger antioxidant activities than other complexes, which show that Cu(II)

Table 7.  Intrinsic binding constant ($K_b$) and change in free energy ($\Delta G$) values for the Ni(II)/Cu(II)–2AB–him, bim, hist, and his complexes ($1.0 \times 10^{-5}$ mol) with variation of CT-DNA (0–100 μM) at room temperature.

| Complex | $\lambda_{max}$ (cm$^{-1}$) | | $\Delta\lambda$ (nm) | Hypochromocity (%) | $K_b \times 10^5$ mol$^{-1}$ | $-\Delta G$ kJ mol$^{-1}$ |
|---|---|---|---|---|---|---|
| | Free | Bound | | | | |
| Complex (1a) | 377 | 382 | 5 | 29.21 | 3.76 | 32.39 |
| Complex (1b) | 376 | 380 | 4 | 31.25 | 5.81 | 33.09 |
| Complex (1c) | 384 | 388 | 4 | 33.09 | 5.28 | 34.21 |
| Complex (1d) | 280, 380 | 284, 383 | 4, 3 | 35.25 | 6.82 | 34.63 |
| Complex (2a) | 285 | 289 | 4 | 15.01 | 4.56 | 33.59 |
| Complex (2b) | 282 | 285 | 3 | 22.58 | 6.19 | 34.38 |
| Complex (2c) | 283 | 288 | 5 | 35.42 | 5.92 | 34.26 |
| Complex (2d) | 286 | 290 | 4 | 40.05 | 7.02 | 34.70 |

complexes could act as excellent chemotherapeutic agents in preventing the progress of aging and treatment of pathological diseases arising from oxidative stress.

### 3.1.9. DNA-binding studies

3.1.9.1. *Electronic absorption study.* Electronic absorption spectra are used to examine the binding interaction of MLB complexes with DNA. The electronic absorption spectrum of Ni(II)/Cu(II)–2AB(L)–him/bim/hist/his(B) complexes in the absence and presence of CT-DNA were studied and the data are given in table 7. A representative absorption spectrum for Ni(II)–2AB(L)–his(B) (**1d**) is shown in figure S3 (Supplementary data file) and Cu(II)–2AB(L)–his(B) (**2d**) is shown in figure 8. Complex **1d** shows two bands in the UV region at 280 and 381 nm. With increasing concentration of CT-DNA, the absorption peaks of the complexes were affected, i.e. the absorption band intensity maximum ($\lambda_{max}$) of charge transfer bands at 280 and 380 ($\varepsilon = 260$–725 dm$^3$ mol$^{-1}$ cm$^{-1}$) nm for **1d** were shifted to longer wavelength (bathochromic shift) along with hypochromism of 25–40% (figure 8). The observed decrease in absorbance with increase in concentration of DNA along with bathochromic shift clearly indicate interaction between the complexes and CT-DNA. Generally, hypochromism and bathochromism indicate that the complexes bind with CT-DNA through an intercalative mode and involve a strong interaction of aromatic chromophore of the complex with the base pairs of DNA [58]. Similar effect (the absorption peak intensity) is observed for the other complexes during the addition of increasing [CT-DNA] under the same experimental conditions. The intrinsic binding constant ($K_b$) is obtained from the ratio of slope to the intercept from the plots of [DNA]/($\varepsilon_a - \varepsilon_f$) *versus* [DNA] and the values are
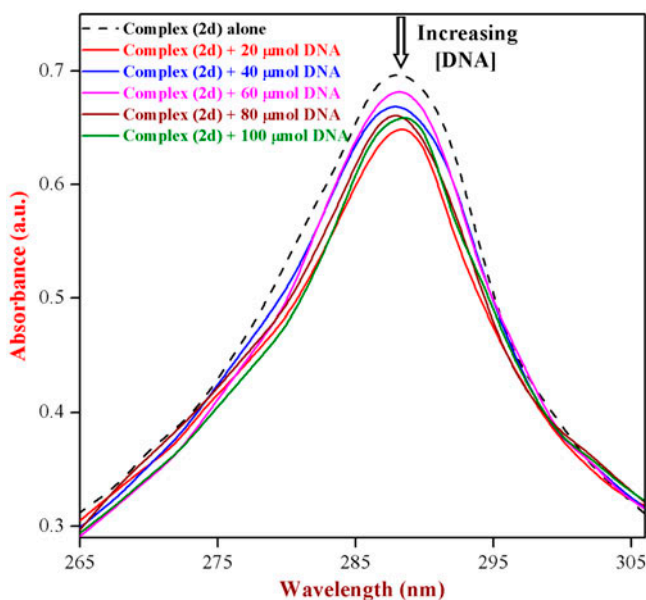


Figure 8. Electronic absorption spectra of Cu(II)–2AB–his complex (**2d**) ($1 \times 10^{-5}$ mol) with the absence (dotted line) and presence (solid line) of CT-DNA at different concentrations in buffer (pH 7.2) medium and the arrow indicates decrease in absorbance intensity upon consecutive addition of CT-DNA.

shown in table 7. From table 7, the trend of $K_b$ values follow the order Cu(II) > Ni(II), which is similar to the trend in Irwing–Williams series; these complexes also show potent antibacterial and antioxidant activities. The $K_b$ values ($4.56 \times 10^5$, $6.19 \times 10^5$, $5.92 \times 10^5$, and $7.02 \times 10^5$ mol$^{-1}$) of

Cu(II) complexes (**2a**–**2d**) agree with some earlier reports of mononuclear Cu(II) complexes [19, 59–61], but these values are much lower than binuclear Cu(II) complexes [61], which is attributed to formation of several hydrogen bonds between the heteroligand complexes and CT-DNA. The $K_b$ values ($4.56 \times 10^5$, $6.19 \times 10^5$, $5.92 \times 10^5$, and $7.02 \times 10^5$ mol$^{-1}$) of Cu(II) complexes (**2a**–**2d**) are consistent with earlier reports on binding of mononuclear Cu(II) complexes with CT-DNA [19, 59–61] and also these values are much lower than dinuclear Cu(II) complexes [61]. The obtained $K_b$ value ($6.19 \times 10^5$ mol$^{-1}$) of **2b** is consistent with similar mononuclear copper(II) complexes having benzimidazole ligands [56] or [Cu(Hptc)(Me$_2$bpy)(H$_2$O)]·3H$_2$O ($6.87 \times 10^3$ mol$^{-1}$) [61], which possess enhanced binding affinity due to the extended aromaticity and coplanarity for better stacking between the base pairs of CT-DNA as well as 2AB(L). The presence of electron-withdrawing amido-NH$_2$ group in the complex will decrease the electron density on the intercalating ligands, reinforcing the attraction between the Cu(II) complex and CT-DNA with the negatively charged phosphate backbone and consequently stabilize the CT-DNA–complex system causing an increase in the DNA-binding affinity [61]. The $K_b$ values are lower than the typical classical intercalators ($K_b$ for EB-DNA, ~$10^6$ mol$^{-1}$), which implies that these complexes bind with CT-DNA relatively less strongly than classical intercalators [19, 59–61]. From the intrinsic binding constant, the change in free energy values ($\Delta G$) were also calculated. The negative free energy changes observed in all cases indicate that the complexes interact with CT-DNA spontaneously [16, 19].
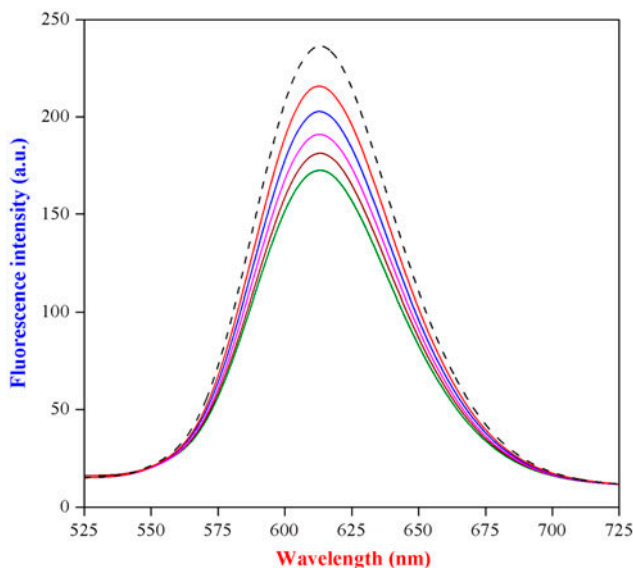


Figure 9. Fluorescence emission spectra of the CT-DNA-EB system ($C_{EB} = 1.0 \times 10^{-5}$ mol) in the absence (dotted line) and presence (solid line) of the Cu(II)–2AB–his complex (**2d**) ($C_{Cu(II) \, complex} = 1 \times 10^{-5}$ mol) with increasing amounts of CT-DNA ($C_{DNA} = 0$, 20, 40, 60, 80, and 100 μmol) in buffer (pH 7.2) medium.

3.1.9.2. *Fluorescence study.* Fluorescence spectra have also been used to study the interaction between the Cu(II) complexes with CT-DNA by measuring the emission intensity of EB bound CT-DNA. The Cu(II)–2AB(L)–him, bim, hist, and his(B) complexes (**2a**–**2d**) exhibited luminescence intensity in Tris–HCl buffer with a maximum wavelength of 618, 608, 615, and 612 nm, respectively, and the representative graph for Cu(II)–2AB(L)–his(B) complex (**2d**) is shown in figure 9. EB is weakly fluorescent and can emit intense fluorescent light in the presence of CT-DNA due to its intercalative binding to DNA [62]. However, this enhanced fluorescence could be quenched or partially quenched by the addition of a second molecule that can replace the bound EB or break the secondary structure of DNA [62]. So, EB can be used as a probe for determination of DNA structure. In this study, the emission spectrum of EB bound DNA in the absence and presence of Cu(II) complexes was recorded. The addition of CT-DNA causes a reduction in emission intensity of ca. 30, 35, 42, and 45% for **2a**, **2b**, **2c**, and **2d**, respectively. This is related to an extent to which the compound penetrates into hydrophobic environment of the DNA, thereby avoiding the quenching of solvent water. The quenching is due to the excited state electron of EB through a photoelectron transfer mechanism. The apparent binding constant ($K_{app}$) values ($5.86 \times 10^5$, $6.22 \times 10^5$, $6.45 \times 10^5$, and $7.25 \times 10^5$ mol$^{-1}$) of **2a**–**2d** are consistent with earlier reports on binding of mononuclear Cu(II) complexes [59–61], suggesting that these Cu(II) complexes bind to CT-DNA through intercalative binding. The obtained $K_{app}$ value of all the Cu(II) complexes are smaller than $K_{EB}$ value ($1.0 \times 10^7$ mol$^{-1}$) which suggests moderate interactions between the Cu(II) complexes and DNA. Also, the results suggest that **2b** and **2d** show better DNA affinity due to the stronger hydrophobic DNA interaction and larger aromaticity.

**3.1.10. Oxidative DNA cleavage activity**. Oxidative DNA cleavage activities of 2AB(L) and its Cu(II)–2AB(L)–him/bim/hist/his(B) complexes (**2a**–**2d**) at 37 °C were studied by gel electrophoresis in the presence of $H_2O_2$ as oxidant. The cleavage properties were studied in Tris–HCl buffer (pH 7.2) and bromophenol blue was used as a photosensitizer. A representative cleavage pictograph of **2a**–**2d** with free 2AB(L) is shown in figure S4 (Supplementary data file). The control experiment using CT-DNA alone (Lane 1) does not show significant cleavage even on longer exposure time. Free radical scavengers inhibited the DNA cleavage, confirming the involvement of free radical. On that basis, a general radical oxidative mechanism is proposed for DNA cleavage, i.e. the M(II) ions react with $H_2O_2$ to produce the diffusible hydroxyl radical (OH·) or molecular oxygen or peroxy derivative via Fenton mechanism or Haber–Weiss mechanism [63]. In oxidative DNA cleavage mechanism, Cu(II) complexes react with $H_2O_2$ to generate the hydroxyl radical (OH·) which abstracts a hydrogen from sugar moiety (at $C_4'$ position) of DNA to form sugar radical and then undergo hydrolytic cleavage at sugar–phosphate backbone to release specific residues depending on the position from which the hydrogen is removed and finally cleaves the DNA [63]. Also, the reaction is modulated by a metallocomplex that binds to a peroxo species generated from the co-reactant $H_2O_2$, which may damage DNA through Fenton-type chemistry [63]. Probably this may be due to the behavior of Cu(II) to form a redox couple in the presence of an oxidant. From the pictograph (figure S4, Supplementary data file), the result clearly indicates that CT-DNA in $H_2O_2$ (Lane 1) and free 2AB(L) in $H_2O_2$ (Lane 2) does not show any significant cleavage, but Cu(II)–2AB(L)–him/his(B) complexes (Lanes 3 and 6) show higher ability to cleave CT-DNA to a considerable extent, whereas other complexes do not cleave the DNA in the presence of oxidant ($H_2O_2$).

**3.1.11. 3D molecular modeling and analysis**. In the present work, the formation of stable six-coordinate M(II)–2AB(L)–his(B) complexes involving monoprotic bidentate 2AB(L) and monoprotic tridentate his(B) ligands were studied and their respective 3D structure of Ni(II) complex is shown in figure S5 (Supplementary data file). The molecular modeling study suggests that all the complexes have distorted octahedral environment. The detailed bond lengths and bond angles of the complexes as per the 3D molecular modeling structure are given in tables S2 and S3 (Supplementary data file), respectively. The arabic numerals were assigned for practicality in favor of the various atoms in the complexes. For each complex, the overall measurements are 93. In most of the complexes, the actual bond lengths and angles are very close to the optimal values which indicate that the proposed geometry of the complexes is accurate but, there are some exceptions.

## 3.2. *Multiple equilibrium studies in solution state*

**3.2.1. Stability and structure of primary M(II)–2AB(L) complexes**. The protonation constants and primary stability constants of M(II)–2AB(L) complexes were determined pH-metrically (pH 2.0–9.0) at 37 °C in 50% (v/v) water–ethanol mixture. From the computer analysis of the pH titration data, HL, $H_2L$, ML, and $ML_2$ species were found in M(II)–2AB (L) complexes and the stability constant values are given in table 8. 2AB(L) offers two well separated buffer regions, due to the successive deprotonation of amine $NH_3^+$ and amide $–CONH_2–$ moieties [41]. In general, the thermodynamically preferred sites for the protonation of amide groups in acidic medium occur only at amido-O [64], whereas the coordination of amido-N takes place only at a very high basic medium (ca. pH ≥ 13) [65, 66] which is not possible in our experimental condition due to increase in the pH (>9.0) level leads to form $[M(OH)_2]$ precipitate. At present experimental condition, the first protonation value of 2-aminobenzamide (−2.41) corresponds to O-amido group which is very close to the reported (−2.67) value [64, 67] and the second (2.67) value corresponds to N-amino group which is low compared to the parent aniline (4.63); this is due to the presence of electron withdrawing amide $(–CONH_2–)$ present in 2AB ligand [68]. No precipitate was observed in the titration vessel which indicates the possibility of $[M(OH)_2]$ formation may be excluded. In the M(II)–2AB(L) system ML and $ML_2$ species are primary (table 8) and complex formation of M(II) ions with 2AB(L) takes place above pH 3, where the ligand predominantly exists only in its neutral form. From table 8, the primary stability constant $(\log \beta_{ML} / \log \beta_{ML_2})$ values clearly show that 2AB(L) is bidentate, i.e. it chelates with M(II) through N-amino (*ortho* to amide $–CONH_2–$ group) and O-amido groups [41] forming stable chelate complexes, similar to M(II)–2-aminobenzoic acid complexes [69]. In $ML_2$ species, both 2AB(L) ligands are bidentate and form six-membered chelate rings with distorted octahedral geometry and this type of binding behavior has already been established in $[M(II)–(2AB)_2–Cl_2]$ complexes in solid state [41]. The protonation and stability constant values of the imidazole containing ligands(B) were redetermined under the same experimental conditions and the calculated values agree with the literature values [18, 70]. These small differences are within the limit of the experimental errors or conditions like ionic strength and temperature effect. From the observed stability constant values (table 8) of M(II)–2AB(L) complexes, the primary 2AB(L) ligand is bidentate, whereas secondary him, bim, hist, and his ligands are mono, mono, bi, and tridentate, respectively. Further, the stability constants of primary complexes (figure 10) follow the trend Zn(II) < Cu(II) > Ni (II) which confirms the Irving–Williams order of stabilities [71]. Also, complex formation

Table 8. Protonation and stability constants of primary M(II) with 2AB, him, bim, hist, and his systems in 50% (v/v) water–ethanol mixture at 37 °C in $I = 0.15$ mol dm$^{-3}$ NaClO$_4$ medium [Error limit: ±0.02–0.06].

| Parameters | Ni(II) | | | | | Cu(II) | | | | | Zn(II) | | | | |
|---|---|---|---|---|---|---|---|---|---|---|---|---|---|---|---|
| | 2AB[a] | him | bim | hist | his | 2AB[a] | him | bim | hist | his | 2AB[a] | him | bim | hist | his |
| $\log \beta_{HB}$ | −2.41 (4) | 7.06(4) | 5.75(5) | 9.81(5) | 9.16(5) | – | – | – | – | – | – | – | – | – | – |
| $\log \beta_{H_2B}$ | 2.75(4) | – | – | 15.69(9) | 15.14(5) | – | – | – | – | – | – | – | – | – | – |
| $\log \beta_{H_3B}$ | – | – | – | – | 17.24(9) | – | – | – | – | – | – | – | – | – | – |
| $\log \beta_{MBH}$ | – | – | – | 11.88(5) | 12.97(7) | – | – | – | 11.84(6) | 13.89(6) | – | – | – | 11.82(4) | 13.08(4) |
| $\log \beta_{MB}$ | 4.31(3) | 3.27(4) | 2.27(6) | 6.32(3) | 8.63(5) | 5.12(2) | 3.32(6) | 2.49(7) | 6.61(5) | 9.64(7) | 3.73(4) | 3.15(5) | 2.14(6) | 6.18(3) | 8.25(2) |
| $\log \beta_{MB_2H}$ | – | – | – | 17.18(7) | 20.69(8) | – | – | – | 17.43(9) | 21.96(9) | – | – | – | 16.89(8) | 20.74(6) |
| $\log \beta_{MB_2}$ | 7.55(5) | 5.55(6) | 4.04(8) | 11.21(5) | 15.76(6) | 9.02(5) | 5.78(8) | 4.28(9) | 11.39(7) | 17.07(8) | 7.01(6) | 5.43(7) | 3.88(9) | 10.98(5) | 15.78(4) |
| $\log \beta_{MB_3}$ | – | 7.74(9) | – | – | – | – | 8.06(9) | – | – | – | – | 7.64(9) | – | – | – |
| $\log \beta_{MB_4}$ | – | 9.51(12) | – | – | – | – | 9.69(11) | – | – | – | – | 9.37(10) | – | – | – |
| $pK^H_{MBH}$ | – | – | – | 5.56 | 4.34 | – | – | – | 5.23 | 4.25 | – | – | – | 5.64 | 4.83 |
| $pK^H_{MB_2H}$ | – | – | – | 5.97 | 4.93 | – | – | – | 6.04 | 4.89 | – | – | – | 5.91 | 4.96 |
| $\log K^M_{MB_2}$ | 3.24 | 2.28 | 1.77 | 4.89 | 7.13 | 3.9 | 2.46 | 1.79 | 4.78 | 7.43 | 3.04 | 2.28 | 1.74 | 4.8 | 7.53 |
| $\log K^{MBH}_{MB_2H}$ | – | – | – | 5.3 | 7.72 | – | – | – | 5.59 | 8.07 | – | – | – | 5.07 | 7.66 |
| $\log K^M_{MB_3}$ | – | 2.19 | – | – | – | – | 2.28 | – | – | – | – | 2.21 | – | – | – |
| $\log K^M_{MB_4}$ | – | 1.77 | – | – | – | – | 1.63 | – | – | – | – | 1.73 | – | – | – |
| $\log P$ | – | – | – | 2.07 | 3.81 | – | – | – | 2.03 | 4.73 | – | – | – | 2.01 | 3.92 |
| $\log K_1/K_2$ | 0.57 | 0.59 | 0.56 | 0.56 | 0.55 | 0.57 | 0.57 | 0.58 | 0.58 | 0.56 | 0.55 | 0.58 | 0.55 | 0.56 | 0.52 |

Note: Standard deviations are given in parentheses.
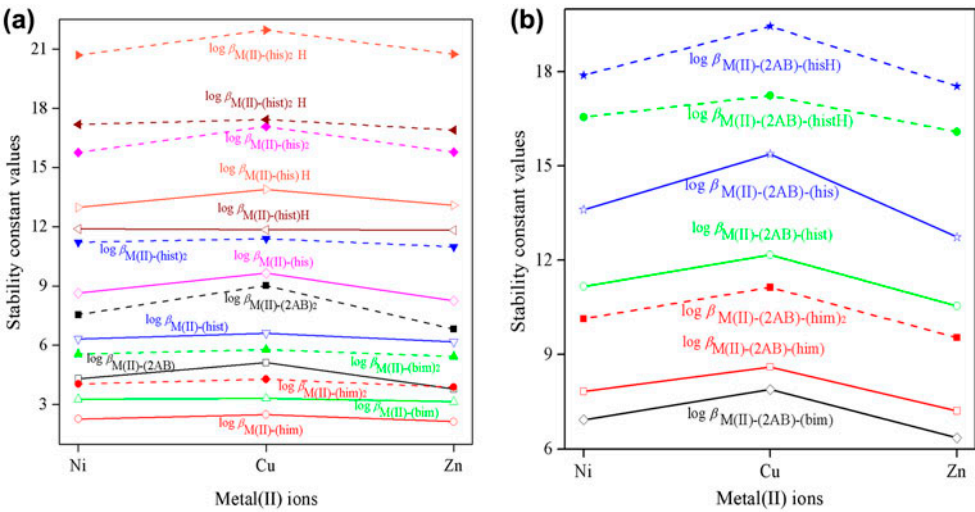[a]2AB: 2-aminobenzamide as a primary ligand(L) in the heteroligand systems.

Figure 10.    Irving–William stability order of (a) primary and (b) heteroligand Ni(II), Cu(II), and Zn(II) systems.

of Ni(II)/Cu(II) with 2AB(L) is accompanied by a sharp color change but the absorbance ($\lambda_{max}$) values do not shift with increasing the pH (2.0–9.0) of the solution. In primary (1 : 5 solution), Ni(II)–2AB(L) complex shows a sharp change in color (pale green) with $\lambda_{max}$ values at 19,724 ($\varepsilon = 350$ dm$^3$ mol$^{-1}$ cm$^{-1}$) and 15,649 cm$^{-1}$ ($\varepsilon = 210$ dm$^3$ mol$^{-1}$ cm$^{-1}$) and

Table 9.    Stability constants and stabilization effects of heteroligand M(II)–2AB–him, bim, hist, and his systems in 50% (v/v) water–ethanol mixture at 37 °C in $I = 0.15$ mol dm$^{-3}$ NaClO$_4$ medium [Error limit: ±0.03–0.05].

| Parameters | Ni(II) | | | | Cu(II) | | | | Zn(II) | | | |
|---|---|---|---|---|---|---|---|---|---|---|---|---|
| | him | bim | hist | his | him | bim | hist | his | him | bim | hist | his |
| $\log\beta_{MLBH}$ | – | – | 16.56 (6) | 17.89 (8) | – | – | 17.24 (5) | 19.45 (7) | – | – | 16.09 (6) | 17.54 (9) |
| $\log\beta_{MLB}$ | 7.83(5) | 6.93 (7) | 11.16 (7) | 13.61 (9) | 8.61(6) | 7.89 (8) | 12.17 (7) | 15.38 (9) | 7.21 (4) | 6.35 (6) | 10.54 (8) | 12.74 (9) |
| $\log\beta_{MLB_2}$ | 10.14 (6) | – | – | – | 11.14 (5) | – | – | – | 9.54 (6) | – | – | – |
| $pK^H_{MLBH}$ | – | – | 5.40 | 4.28 | – | – | 5.07 | 4.07 | – | – | 5.55 | 4.80 |
| $\log K^{ML}_{MLBH}$ | – | – | 12.25 | 13.58 | – | – | 12.12 | 14.33 | – | – | 12.31 | 13.76 |
| $\log K^{MBH}_{MLBH}$ | – | – | 4.68 | 4.92 | – | – | 5.40 | 5.56 | – | – | 4.27 | 4.46 |
| $\log K^{ML}_{MLB}$ | 3.52 | 2.62 | 6.85 | 9.30 | 3.49 | 2.77 | 7.05 | 10.26 | 3.43 | 2.57 | 6.76 | 8.96 |
| $\log K^{MB}_{MLB}$ | 4.56 | 4.66 | 4.84 | 4.98 | 5.29 | 5.40 | 5.56 | 5.74 | 4.06 | 4.21 | 4.36 | 4.49 |
| $\log K^{ML}_{MLB_2}$ | 5.83 | – | – | – | 6.02 | – | – | – | 5.76 | – | – | – |
| $\log K^{MB_2}_{MLB_2}$ | 4.59 | – | – | – | 5.36 | – | – | – | 4.11 | – | – | – |
| $\Delta\log K_{MLBH}$ | – | – | 0.37 | 0.61 | – | – | 0.28 | 0.44 | – | – | 0.49 | 0.68 |
| $\Delta\log K_{MLB}$ | 0.25 | 0.35 | 0.53 | 0.67 | 0.17 | 0.28 | 0.44 | 0.62 | 0.28 | 0.43 | 0.58 | 0.71 |
| $\Delta\log K_{MLB_2}$ | 0.28 | – | – | – | 0.24 | – | – | – | 0.33 | – | – | – |
| $\log X$ | 1.35 | 1.06 | 2.35 | 2.70 | 2.68 | 2.74 | 4.19 | 4.93 | 2.17 | 2.00 | 3.28 | 2.88 |
| $\log X'$ | 0.71 | 0.81 | 0.99 | 1.13 | 1.44 | 1.55 | 1.71 | 1.89 | 1.02 | 1.17 | 1.32 | 1.45 |
| %R.S. | 7.65 | 15.42 | 8.39 | 7.76 | 5.12 | 11.24 | 6.66 | 6.43 | 8.89 | 20.09 | 9.39 | 8.61 |

Note: Standard deviations are given in parenthesis.

these absorption bands may be assigned to $^1A_{1g} \rightarrow {}^1B_{1g}$ and $^1A_{1g} \rightarrow {}^1A_{2g}$ transitions, respectively, with square-planar environment [43]. Also, the primary Cu(II) complex is deep blue at pH 6.5 with $\lambda_{max}$ value at 36,363 ($\varepsilon = 820$ dm$^3$ mol$^{-1}$ cm$^{-1}$) and 15,361 cm$^{-1}$ ($\varepsilon = 185$ dm$^3$ mol$^{-1}$ cm$^{-1}$) which can be assigned to $L \rightarrow M$ charge transfer and $^2B_{1g} \rightarrow {}^2A_{1g}$ transitions, respectively, also supporting square-planar geometry [16, 43].

**3.2.2. Stability and structure of heteroligand complex equilibria**. The pH-metric data illustrate formation of MLBH, MLB, and MLB$_2$ species in addition to various primary HL, H$_2$L, ML, ML$_2$, HB, H$_2$B, MBH, MB, MB$_2$H, and MB$_2$ species. The stability constant values for the heteroligand complexes are reported in table 9. In the present work, the experiment was carried out from 2.0 to 9.0 pH and in the increasing pH level (pH > 9.0), the title complexes undergo hydroxylation to form [M(OH)$_2$] precipitate. To characterize the stability of heteroligand equilibria with respect to their corresponding primary analogs the terms $\Delta \log K$, $\log X$, $\log X'$, and %R.S. are used.

*3.2.2.1. Stability and structure of MLB and MLB$_2$ species.* The formation of MLB [M = Ni (II)/Cu(II)/Zn(II); L = 2AB and B = him/bim/hist/his] speices has been found in the pH range of 4.5–7.0 and there is a steady increase in formation with rise of pH. The obtained $\log K_{MLB}^{MB}$ values (table 9) in M(II)–2AB(L)–imidazoles(B) complex is comparable with $\log K_{ML}^M$ values in M(II)–2AB complexes (table 8) which indicate that similar binding of 2AB in the MLB species, i.e. 2AB(L) is bidentate, chelating with M(II) ions via amino-N and amide-O in MLB species. Again, $\log K_{MLB}^{ML}$ for the M(II)–2AB–him, bim, hist, and his complexes (table 9) compare favorably with $\log K_{MB}^M$ values in the M(II)–imidazoles complexes (table 8), demonstrating monodentate binding of him/bim, bidentate binding of hist and tridentate binding of his in their respective MLB species. Thus, the three coordinating positions of MLB species in the M(II)–2AB–him/bim complexes would be occupied by binding of bidentate 2AB and monodentate him/bim. The remaining position would be completed by solvent water. Also, the higher stability for the MLB complexes containing him compared to that of bim can be ascribed due to the higher basicity of him ligand. The $\log \beta_{MLB}$ values in the M(II)–2AB–his complexes are higher than that in the corresponding hist complexes which clearly indicate the tridentate binding of his in the MLB species. The binding of hist and his in the MLB species in the presence of 2AB involves six–six and six–five–six membered chelate rings, respectively. The formation of later chelate ring complexes would be preferred due to the fact that the rings of different sizes introduce more ligand field asymmetry and stabilize the heteroligand complexes. In order to study the stabilization of MLB species with respect to their primary viz., (i) $\Delta \log K_{MLB} [= \log \beta_{MLB} - (\log \beta_{ML} + \log \beta_{MB})]$ and (ii) disproportionation constant $\log X_{MLB} [= 2\log \beta_{MLB} - (\log \beta_{ML_2} + \log \beta_{MB_2})]$ values. In general, the statistically [72–74] expected $\Delta \log K$ values for regular octahedral and square planar geometries are −0.4 and −0.6, respectively. From table 9, the calculated $\Delta \log K_{MLB}$ values for all the complexes are more positive than the statistically expected values [72–74], which indicate the higher stabilization of the heteroligand complexes than their primary analogs, i.e. the secondary ligands(B) preferred to add to M(II)–2AB primary complexes rather than to aquated M(II) complexes. The $\log X$ values for all the complexes are much higher than statistical (+0.6) [75] value, which demonstrate that the interligand electronic and steric interactions are present in the heteroligand complexes. Moreover, the calculated $\log X'$ values are greater than statistical (0.3), suggesting

that the formation of MLB complexes is preferred over their primary $ML_2$ or $MB_2$ complexes. The relative stabilization [76, 77] $\left[ \%\text{R.S.} = \frac{(\log K_{\text{MLB}}^{\text{ML}} - \log K_{\text{MB}}^{\text{M}})}{(\log K_{\text{MB}}^{\text{M}})} \times 100 \right]$ values are used to determine the relative stabilization for the different heteroligand complexes and the observed %R.S. values indicate the marked stabilization of MLB complexes. From table 9, the MLB complexes follow the Irving–William stability order: NiLB < CuLB > ZnLB (figure 10) and their stability constants are M(II)–2AB–his > M(II)–2AB–hist > M(II)–2AB–him > M(II)–2AB–bim.

Moreover, the formation of Ni(II)/Cu(II)–2AB–imidazole complexes are accompanied by a sharp color change of the medium but the absorbance ($\lambda_{\text{max}}$) values do not shift with increasing the pH (3.0–9.0) of the solution. The electronic spectra of Ni(II)–2AB–him/bim/hist/his complexes (1 : 1 : 1) display three spin-allowed d–d transitions (table 3) at 10,864–11,135 cm$^{-1}$ ($\varepsilon = 78$ dm$^3$ mol$^{-1}$ cm$^{-1}$), 16,153–18,920 cm$^{-1}$ ($\varepsilon = 165$ dm$^3$ mol$^{-1}$ cm$^{-1}$), and 22,455–26,840 cm$^{-1}$ ($\varepsilon = 280$ dm$^3$ mol$^{-1}$ cm$^{-1}$), which may be due to $^3A_{2g}$ (F) $\rightarrow$ $^3T_{2g}$ (F), $^3A_{2g}$ (F) $\rightarrow$ $^3T_{1g}$ (F), and $^3A_{2g}$ (F) $\rightarrow$ $^3T_{1g}$ (P) transitions, respectively, with distorted octahedral geometry with $^3A_{2g}$ as ground state [43]. Absence of any band below 10,000 cm$^{-1}$ ruled out the possibility of a tetrahedral environment around the Ni(II) ion. Also, the Cu(II)–2AB–him/bim/hist/his complexes (1 : 1 : 1) exhibit moderate Jahn–Teller distortion with only one broad and unsymmetrical absorption band centered at 14,677, 14,246, 14,359, and 14,781 cm$^{-1}$ ($\varepsilon = 140$–165 dm$^3$ mol$^{-1}$ cm$^{-1}$), respectively, which may be assigned to $^2E_g \rightarrow {}^2T_{2g}$ transition with distorted octahedral geometry [43].

In the case of M(II)–2AB–him complexes, the formed MLB$_2$ species [M = Ni(II)/Cu(II)/Zn(II); L = 2AB and B = him], the solvent water molecules of MLB species would be replaced by a second imidazole ligand. The $\log K_{\text{MLB}_2}^{\text{MB}_2}$ and $\log K_{\text{MLB}_2}^{\text{ML}}$ values (table 9) in the M(II)–2AB–him complexes are comparable with $\log K_{\text{ML}}^{\text{M}}$ and $\log K_{\text{MB}_2}^{\text{M}}$ values in the primary complexes (table 8) and the MLB$_2$ species in the M(II)–2AB–him complexes would be four-coordinate due to bidentate binding of 2AB and monodentate binding of two molecules of him. Also, the $\log \beta_{\text{MLB}}$ values in the M(II)–2AB–hist complexes are much higher than the $\log \beta_{\text{MLB}_2}$ values of the M(II)–2AB–him complexes, where in both complexes the metal (II) ions have the same type of coordination. This enhanced stability observed in the former complex is from the chelate effect of hist ligand in the complexes.

3.2.2.2. *Stability and structure of MLBH complexes.* The formed protonated MLBH species [M = Ni(II)/Cu(II)/Zn(II); L = 2AB and BH = histH/hisH] for M(II)–2AB–hist/his complexes have been favored from pH 4.0–5.5. In M(II)–2AB complexes, there is no protonated primary species while monoprotonated primary species have been detected in M(II)–hist/his complexes (table 8). The $pK_{\text{MLBH}}^{\text{H}}$ values obtained in M(II)–2AB–hist/his complexes follow the same trends of the respective $pK_{\text{MBH}}^{\text{H}}$ values in the M(II)–hist/his complexes (table 8). This demonstrates the possibility of attachment of an extra proton with secondary ligands, possibly to its amino group as in the case of MBH in hist and his complexes. This is further supported by the obtained $\log K_{\text{MLBH}}^{\text{ML}}$ values (table 9) thus, these complexes are comparable to the $\log K_{\text{MBH}}^{\text{M}}$ values in the primary M(II)–hist/his complexes. From table 9, the calculated $\Delta \log K_{\text{MLBH}}$ values for all the heteroligand complexes are more positive when compared to the statistical values [72–74], which indicate noticeable stabilization of the protonated MLBH complexes.
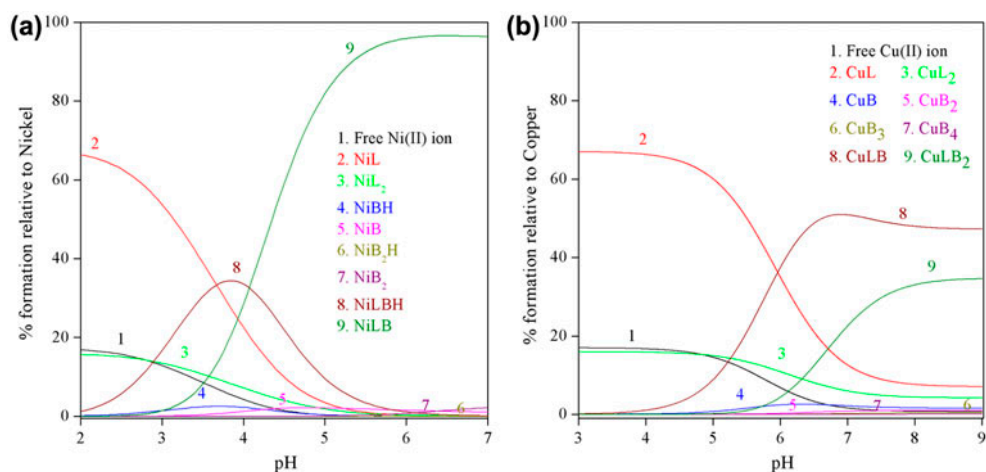
Figure 11. Species distribution diagram of (a) Ni(II)–2AB–his system (1 : 1 : 1) and (b) Cu(II)–2AB–him system (1 : 1 : 2) in 50% (v/v) water–ethanol mixture at 37 °C.

**3.2.3. Species distribution diagram**. Species distribution diagram for all the complexes under the present investigation have been obtained for different M(II) ions to L and B ratios in solution. With increase of pH (≥4.5), the formations of MLB complexes were preferred, up to 85–95% of the total metal(II) ions. High stability of six- and five-membered chelates when compared to six and six has also been reflected in the species distribution diagram. In all the complexes, the primary ML and $ML_2$ complexes were ~30–65% whereas the MBH, MB, $MB_2H$, $MB_2$, $MB_3$, and $MB_4$ species accounted for ~10–20% of the total metal(II) ions. At lower pH ranges (4.0–5.5), the MLBH species have been found and accounted for ~25–45%. The $MLB_2$ species in M(II)–2AB–him complexes are favored above pH 6.0 and accounted for 25–40% of the total M(II) ions in 1 : 1 : 2 solutions. In order to show these qualitative trends found in the species distribution plots, the diagrams obtained for the Ni (II)–2AB–his and Cu(II)–2AB–him complexes are shown in figure 11.

## 4. Conclusion

We synthesized bioactive MLB complexes characterized using various spectral techniques. The PXRD and SEM analysis show that these complexes display sharp crystalline peaks with well-defined microcrystalline nature with an average grain size of 35–41 nm and homogeneous particle nature. All the heteroligand complexes under investigation show octahedral environment around the central M(II) ions. *In vitro* biological activities of the MLB complexes show more potent antimicrobial activities than free 2-aminobenzamide ligand in different micro-organisms. Oxidative CT-DNA cleaving activities of 2AB and CuLB heteroligand complexes under aerobic conditions show moderate activity. Biological and antioxidant studies confirmed that MLB complexes show better biological and antioxidant properties than free 2AB. Furthermore, the stability of Ni(II)/Cu(II)/Zn(II) heteroligand complexes involving 2AB and some imidazole containing enzyme constituents (him, bim,

hist, and his) in 50% (v/v) water–ethanol at 37 °C and $I = 0.15$ mol dm$^{-3}$ (NaClO$_4$) were determined. In MLBH/MLB/MLB$_2$ species of M(II)–2AB–him/bim/hist/his complexes, 2AB binds bidentate, whereas him/bim/hist/his are mono, mono, bi, and tridentate, respectively. In MLBH species of M(II)–2AB–hist/his complexes, the extra proton resides with hist/his. The results indicate that the heteroligand complexes have higher stability than their corresponding primary analogs. The percentage distribution of various primary and heteroligand species in solution has also been evaluated.

## Acknowledgements

## Disclosure statement

## Supplemental data

## References

[1] K. Burger. *Biocoordination Chemistry: Coordination Equilibria in Biologically Active Systems*, Ellis Horwood, New York (1990).
[2] M.S.S. Babu, P.G. Krishna, K.H. Reddy, G.H. Philip. *Indian J. Chem.*, **47A**, 1661 (2008).
[3] N. Farrell. *Transition Metal Complexes as Drugs and Chemotherapeutic Agents*, Kluwer Academic, Dordrecht (1989).
[4] M.H. Habibi, E. Shojaee, M. Ranjbar, H.R. Memarian, A. Kanayama, T. Suzuki. *Spectrochim. Acta, Part A*, **105**, 563 (2013).
[5] F. Fiorino, M. Eiden, A. Giese, B. Severino, A. Esposito, M.H. Groschup, E. Perissutti, E. Magli, G.M. Incisivo, A. Ciano, F. Frecentese, H.A. Kretzschmar, J. Wagner, V. Santagada, G. Caliendo. *Bioorg. Med. Chem.*, **20**, 5001 (2012).
[6] D. Oltmanns, M. Eisenhut, W. Mier, U. Haberkorn. *Curr. Med. Chem.*, **16**, 2086 (2009).
[7] H. Hou, M. Tian, H. Zhang. *Anat. Rec.*, **295**, 722 (2012).
[8] P. Zhang, L. Bao, J.F. Zuckett, E.A. Goldman, Z.J. Jia, A. Arfsten, S. Edwards, U. Sinha, A. Hutchaleelaha, G. Park, J.L. Lambing, S.J. Hollenbach, R.M. Scarborough, B.Y. Zhu. *Bioorg. Med. Chem. Lett.*, **14**, 983 (2004).
[9] L. Royle, T.S. Mattu, E. Hart, J.I. Langridge, A.H. Merry, N. Murphy, D.J. Harvey, R.A. Dwek, P.M. Rudd. *Anal. Biochem.*, **304**, 70 (2002).
[10] H. Sigel. *Metal Ions in Biological Systems*, Vol. 1–37, M. Dekker, New York (1971–1997).

[11] S. Liu, W. Gu, D. Lo, X.Z. Ding, M. Ujiki, T.E. Adrian, G.A. Soff, R.B. Silverman. *J. Med. Chem.*, **48**, 3630 (2005).
[12] J.R.F. Silva, R.J.P. Williams. *The Biological Chemistry of the Elements; The Inorganic Chemistry of the Life*, Clarendon Press, Oxford (1991).
[13] K. Starčević, M. Kralj, K. Ester, I. Sabol, M. Grce, K. Pavelić, G.K. Karminski-Zamola. *Bioorg. Med. Chem.*, **15**, 4419 (2007).
[14] H.T. Chifotides, K.R. Dunbar. *Acc. Chem. Res.*, **38**, 146 (2005).
[15] R. Bonnet. *Chemical Aspects of Photodynamic Therapy*, Gordon and Breach Science Publishers, London (2000).
[16] J. Dharmaraja, T. Esakkidurai, P. Subbaraj, S. Shobana. , *Spectrochim. Acta, Part A*, **114**, 607 (2013).
[17] J. Dharmaraja, P. Subbaraj, T. Esakkidurai, S. Shobana. *Spectrochim. Acta, Part A*, **132**, 604 (2014).
[18] J. Dharmaraja, P. Subbaraj, T. Esakkidurai, S. Shobana, S. Raji. *Acta Chim. Slov.*, **61**, 803 (2014).
[19] S. Shobana, J. Dharmaraja, S. Selvaraj. *Spectrochim. Acta, Part A*, **107**, 117 (2013).
[20] P. Subbaraj, A. Ramu, N. Raman, J. Dharmaraja. *J. Coord. Chem.*, **67**, 2747 (2014).
[21] D.D. Perrin, W.L.F. Armarego, D.R. Perrin. *Purification of Laboratory Chemicals*, Pergamon Press, Oxford (1980).
[22] G. Gran. *Analyst*, **77**, 661 (1952).
[23] A. Earnshaw. *Introduction to Magnetochemistry*, Academic Press, New York (1968).
[24] *CS Chem 3D Ultra Molecular Modeling and Analysis*, Cambridge, www.cambridgesoft.com.
[25] M.J. Pelczar, E.C.S. Chan, N.R. Krieg. *Microbiology*, 5th Edn, Tata McGraw Hill Publishing Co. Ltd., New Delhi (1998).
[26] M.S. Blois. *Nature*, **181**, 1199 (1958).
[27] J. Marmur. *J. Mol. Biol.*, **3**, 208 (1961).
[28] J.K. Barton. *Science*, **223**, 727 (1986).
[29] S. Sortino, G. Condorelli. *New J. Chem.*, **26**, 250 (2002).
[30] A. Wolfe, G.H. Shimer Jr., T. Meehan. *Biochemistry*, **26**, 6392 (1987).
[31] S. Zhang, J. Zhou. *J. Coord. Chem.*, **61**, 2488 (2008).
[32] H.M. Irving, M.G. Miles, L.D. Pettit. *Anal. Chim. Acta*, **38**, 475 (1967).
[33] I.G. Sayce. *Talanta*, **18**, 653 (1971).
[34] L.G. Uitert, C.G. Haas. *J. Am. Chem. Soc.*, **75**, 451 (1953).
[35] N. Durust, M.A. Akay, Y. Durest, E. Kilic. *Anal. Sci.*, **16**, 825 (2000).
[36] L. Alderighi, P. Gans, A. Ienco, D. Peters, A. Sabatini, A. Vacca. *Coord. Chem. Rev.*, **184**, 311 (1999).
[37] W.J. Geary. *Coord. Chem. Rev.*, **7**, 81 (1971).
[38] K. Nakamoto. *Infrared and Raman Spectra of Inorganic and Coordination Compounds*, Wiley, New York (1986).
[39] J.R. Ferraro. *Low-frequency Vibrations of Inorganic and Coordination Compounds*, Plenum Press, New York (1971).
[40] L.J. Bellamy, *The Infrared Spectra of Complex Molecules*, 2nd Edn, Chapman &Hall, Methuen (1958).
[41] J.R. Allan, B. McCloy, A.D. Paton, W.E. Smith, D.L. Gerrard. *Thermochim. Acta*, **205**, 127 (1992).
[42] R.L. Dutta, A. Syamal. *Elements of Magnetochemistry*, 2nd Edn, East-West Press, New Delhi (1992).
[43] A.B.P. Lever. *Electronic Spectra of dn Ions in Inorganic Electronic Spectroscopy*, 2nd Edn, Elsevier, Amsterdam (1984).
[44] C.J. Ballhausen, *Introduction to Ligand Field Theory*, McGraw-Hill, New York (1962).
[45] B.N. Figgis, M.A. Hitchman, *Ligand Field Theory and Its Applications*, Wiley-VCH, New York (2000).
[46] B.R. McGarvey. In *Transition Metal Chemistry*, R.L. Carlin (Ed.), Marcel Dekker, New York (1966).
[47] A.W. Addison. In *Copper Coordination Chemistry: Biochemical and Inorganic Perspectives*, K.D. Karlin, J.A. Zubieta (Ed.), Adenine Press, Guilderland, NY (1983).
[48] B.J. Hathaway, D.E. Billing. *Coord. Chem. Rev.*, **5**, 143 (1970).
[49] W.W. Simons. *The Sadtler Handbook of Proton NMR Spectra*, Sadtler Research Laboratories, Philadelphia, PA (1978).
[50] B.D. Cullity. In *Elements of X-ray Diffraction*, M. Cohen (Ed.), 2nd Edn, Addison-Wesley Publishing Company Inc., Philippines (1978).
[51] M.A. Estermann, W.I.F. David. In *Structure Determination from Powder Diffraction Data (SDPD)*, W.I.F. David, K. Shankland, B. McCusker, Ch. Baerlocher (Eds.), Oxford Science Publications, New York (2002).
[52] J. Goldstein, D. Newbury, D. Joy, C. Lyman, P. Echlin, E. Lifshin, L. Sawyer, J. Michael. *Scanning Electron Microscopy and X-ray Microanalysis*, 3rd Edn, Kluwer Academic, Plenum Publishers, New York (2003).
[53] Y. Anjaneyulu, R.P. Rao. *Synth. React. Inorg. Met.-Org. Chem.*, **16**, 257 (1986).
[54] B.G. Tweedy. *Phytopathology*, **55**, 910 (1964).
[55] S.B. Bukhari, S. Memon, M. Mahroof-Tahir, M.I. Bhanger. *Spectrochim. Acta, Part A*, **71**, 1901 (2009).
[56] H. Wu, J. Zhang, Y. Zhang, C. Chen, Z. Li, M. Wu, Z. Yang. *J. Coord. Chem.*, **68**, 835 (2015).
[57] Z.L. Hua, W.W. Na, W. Yuan, S. Guang. *J. Coord. Chem.*, **66**, 227 (2013).
[58] S. Zhang, J. Zhou. *J. Coord. Chem.*, **61**, 2488 (2008).
[59] J. Lakshmipraba, S. Arunachalam, R.V. Solomon, P. Venuvanalingam. *J. Coord. Chem.*, **68**, 1374 (2015).

[60] R.K.B. Devi, S.P. Devi, R.K.B. Singh, R.K.H. Singh, T. Swu, W.R. Devi, C.H.B. Singh. *J. Coord. Chem.*, **67**, 891 (2014).
[61] X.L. Wang, M. Jiang, Y.T. Li, Z.Y. Wu, C.W. Yan. *J. Coord. Chem.*, **66**, 1985 (2013).
[62] Y.F. Song, P. Yang. *Polyhedron*, **20**, 501 (2001).
[63] T.D. Tullius (Ed.). *Metal-DNA Chemistry, ACS Symposium Series 402*, American Chemical Society, Washington, DC (1989).
[64] R.B. Homer, C.D. Johnson. In *Acid–base and Complexing Properties of Amides*, J. Zabicky (Ed.), Chap. 3, John Wiley & Sons Ltd., New York (2010).
[65] H. Sigel, R.B. Martin. *Chem. Rev.*, **82**, 385 (1982).
[66] D. Chen, Y. Sun, A.E. Martell, M.J. Welch. *Inorg. Chim. Acta*, **335**, 119 (2002).
[67] B. Garcia, R.M. Casado, J. Castillo, S. Ibeas, I. Domingo, J.M. Leal. *J. Phys. Org. Chem.*, **6**, 101 (1993).
[68] Z.Z. Rappoport. *The Chemistry of Anilines*, John Wiley & Sons Ltd., The Atrium (2007).
[69] D.L. Dinsel, T.R. Sweet. *Anal. Chem.*, **35**, 2077 (1963).
[70] S. Sjoberg. *Pure Appl. Chem.*, **69**, 1549 (1997).
[71] H. Irving, R.J.P. Williams. *J. Chem. Soc.*, **8**, 3192 (1953).
[72] H. Sigel. In *IUPAC Coordination Chemistry-20*, D. Banerjea (Ed.), Pergamon Press, Oxford (1980).
[73] L.G. Sillen, A.E. Martell. *Stability Constants of Metal-Ion complexes*, Supplement, Special Publication, Royal Society of Chemistry, Great Britain (1971).
[74] H. Sigel. *Angew. Chem. Int. Ed.*, **14**, 394 (1975).
[75] R. Dewitt, J.I. Watters. *J. Am. Chem. Soc.*, **76**, 3810 (1954).
[76] S.N. Limaye, M.C. Saxena. *J. Indian Chem. Soc.*, **61**, 448 (1984).
[77] S.N. Limaye, M.C. Saxena. *J. Indian Chem. Soc.*, **62**, 576 (1985).